Plasma Sci. Technol. **26** (2024) 053001 (16pp) https://doi.org/10.1088/2058-6272/ad15e0

Nonlinear dynamics of the reversed shear Alfvén eigenmode in burning plasmas

Tao WANG (王涛)[1,2], **Shizhao WEI** (魏士朝)[1,‡], **Sergio BRIGUGLIO**[3], **Gregorio VLAD**[3], **Fulvio ZONCA**[2,3,1] **and Zhiyong QIU** (仇志勇)[1,2,*]

[1] Institute for Fusion Theory and Simulation and School of Physics, Zhejiang University, Hangzhou 310027, People's Republic of China
[2] Center for Nonlinear Plasma Science, ENEA C.R. Frascati, Frascati 00044, Italy
[3] Fusion and Nuclear Safety Department, ENEA C.R. Frascati, Frascati 00044, Italy

[*]E-mail of corresponding author: zqiu@zju.edu.cn

Received 12 September 2023, revised 8 December 2023
Accepted for publication 12 December 2023
Published 25 April 2024

Abstract

In a tokamak fusion reactor operated at steady state, the equilibrium magnetic field is likely to have reversed shear in the core region, as the noninductive bootstrap current profile generally peaks off-axis. The reversed shear Alfvén eigenmode (RSAE) as a unique branch of the shear Alfvén wave in this equilibrium, can exist with a broad spectrum in wavenumber and frequency, and be resonantly driven unstable by energetic particles (EP). After briefly discussing the RSAE linear properties in burning plasma condition, we review several key topics of the nonlinear dynamics for the RSAE through both wave-EP resonance and wave-wave coupling channels, and illustrate their potentially important role in reactor-scale fusion plasmas. By means of simplified hybrid MHD-kinetic simulations, the RSAEs are shown to have typically broad phase space resonance structure with both circulating and trapped EP, as results of weak/vanishing magnetic shear and relatively low frequency. Through the route of wave-EP nonlinearity, the dominant saturation mechanism is mainly due to the transported resonant EP radially decoupling with the localized RSAE mode structure, and the resultant EP transport generally has a convective feature. The saturated RSAEs also undergo various nonlinear couplings with other collective oscillations. Two typical routes as parametric decay and modulational instability are studied using nonlinear gyrokinetic theory, and applied to the scenario of spontaneous excitation by a finite amplitude pump RSAE. Multiple RSAEs could naturally couple and induce the spectral energy cascade into a low frequency Alfvénic mode, which may effectively transfer the EP energy to fuel ions via collisionless Landau damping. Moreover, zero frequency zonal field structure could be spontaneously excited by modulation of the pump RSAE envelope, and may also lead to saturation of the pump RSAE by both scattering into stable domain and local distortion of the continuum structure.

Keywords: reversed shear Alfvén eigenmode, energetic particle, nonlinear gyrokinetic theory, saturation, burning plasma

(Some figures may appear in colour only in the online journal)

1. Introduction

The shear Alfvén wave (SAW), described by the dispersion relation $\omega_A^2 = k_\parallel^2 v_A^2$, is a fundamental branch of electromagnetic fluctuations in strongly magnetized plasmas [1]. Here, $k_\parallel$ is the wavenumber parallel to the equilibrium magnetic field $\boldsymbol{B}_0$, and $v_A = B_0/\sqrt{4\pi n_i m_i}$ is the Alfvén speed. The particular interest on the SAW in magnetic fusion research, is mainly due to the possibility that they can be resonantly

[‡]Present address: National Institute for Fusion Science, Toki, Gifu 509-5292, Japan

[*] Author to whom any correspondence should be addressed.

driven unstable by energetic particles (EP) [2], notably alpha particles born from D-T fusion reactions and fast ions/electrons generated by external heating. In turn, finite amplitude SAW fluctuations induce anomalous EP transport, which could degrade the heating and current drive efficiency [3] and possibly damage the plasma facing components [4]. Indeed, significant unmitigated EP redistribution cannot be tolerated in self-sustained burning plasmas such as the ITER [5]. Thus, understanding the linear property, nonlinear saturation and further evolution, as well as the eventual consequences of the EP-driven SAW fluctuation is crucial for achieving burning plasmas in the next generation devices. A thorough theoretical review on the SAW and EP dynamics is given by Chen and Zonca [2], where a generalized fishbone-like dispersion relation (GFLDR) theoretical framework is developed. The present brief review may be considered as an application or elaboration of this general theoretical framework, focusing on a specific SAW branch expected to be important in reactor-scale burning plasmas, namely, the reversed shear Alfvén eigenmode (RSAE) [6, 7].

In confined fusion plasmas, the profile nonuniformity and magnetic geometry render the SAW spectrum continuously varying radially as a continuum $\omega_A(r)$ [8]. A SAW fluctuation may be continuum damped as it resonantly interacts with the SAW continuum [9] by mode conversion to short scale kinetic Alfvén wave (KAW) [10, 11] whose perpendicular wavelength is of the ion Larmor radius ρ_i scale, and is eventually Landau damped by mainly electrons [10, 11]. Thus, the SAW excitation is usually suppressed unless the EP drive is strong enough to overcome the threshold associated with the continuum damping, or the continuum damping can be minimized due to, e.g., the existence of frequency gaps in the SAW continuum. The corresponding modes are, respectively, the EP continuum mode (EPM) [12] and various branches of Alfvén eigenmode (AE), such as the toroidal AE (TAE) [13] inside toroidal periodicity induced frequency gap [14], and the β-induced AE (BAE) [15, 16] associated with finite plasma compressibility with β the thermal to magnetic pressure ratio. Figure 1(a) gives a schematic illustration of a typical SAW continuum in normal (positive) sheared plasma, as well as rough locations of the TAE and BAE gaps. Here, $s = (r/q)\partial_r q$ denotes the magnetic shear with q the safety factor. In addition to these ideal MHD SAW eigenmodes, when the kinetic effects, including ion finite Larmor radius (FLR) effect, finite electron inertia and/or resistivity are considered, a multitude of their KAW counterpart also exist with narrow radial structures and discretized frequency spectrum inside the continuum [2, 17–20], such as kinetic TAE [17, 18] and kinetic BAE [21].

Besides the gap modes, another possibility for the AE to elude significant continuum damping is where the gradient $\partial_r \omega_A$ vanishes, usually nearby the flux surface where the q profile reaches a local extremum (generally minimum, labelled as q_{min}), figure see 1(b) for a comparison. Since the existence of q extrema implies that a radial region is characterized by reversed (negative) shear, the corresponding AE has been dubbed RSAE [22, 23]. Note that in addition to

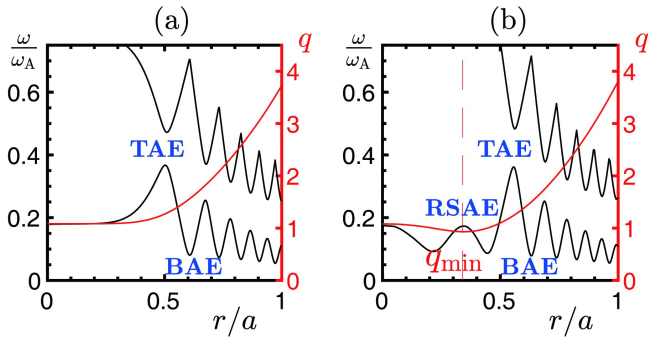

Figure 1. Illustrative viewgraphs of the q profile (red, right axis) and the corresponding SAW continuum ω_A (black, left axis) in positive shear (a) and reversed shear (b) tokamak plasmas, the location of q_{min} is indicated in (b) as a dashed vertical line.

minimizing the continuum damping, various other effects contribute to form an effective potential well within which a localized eigenmode exists as a bound state nearby q_{min}, including toroidicity [24], the curvature of q profile (i.e., $\partial_r^2 q$ at q_{min}) [7], finite Larmor radius effect of EP [25], plasma pressure gradient [26], and kinetic effects [27]. Interested readers may refer to [28] for a detailed simulation illustration on the RSAE existence criteria. Combining all these factors, experimentally, the RSAEs are most easily excited by large-orbit energetic ions during the current ramp-up stage, where the nonmonotonic q profile is (sometimes temporarily) created by insufficient current penetration [29]. For certain poloidal/toroidal mode numbers m/n, a RSAE often exhibits a signature frequency up-sweeping behavior from BAE ($k_\parallel q_{min} R_0 \simeq n q_{min} - m \simeq 0$, R_0 is the major radius) to TAE ($k_\parallel q_{min} R_0 \simeq -1/2$) frequency ranges, when q_{min} decreases from a rational value, while down-sweeping RSAEs below [30, 31] or above [32] the TAE frequency with different ranges of $k_\parallel$ have also been reported. The linear physics of RSAE and its implication to experimental diagnostics have been reviewed in section 2 of [33], and will not be elaborated here. Instead, we mostly focus on the nonlinear dynamics of the RSAE.

Our interest in the RSAE originates from the expectation that burning plasma operations in future tokamak devices, such as ITER [34], CFETR [35], SPARC [36], will likely involve reversed shear. In fact, an economical reactor should operate as much as possible at a self-organized steady state with sustained fusion burning. Thus, besides the fundamental requirement that alpha particles are well confined and their energy can be efficiently channelled to the fuel ions [37], the plasma current should be maintained noninductively, where the self-generated bootstrap current is generally considered as the main component [38]. Note that the radial profile of the bootstrap current peaks off-axis since it is related with the plasma pressure gradient [39], and, thus, a fully noninductive scenario is commonly characterized by reversed magnetic shear. Indeed, the first experimental identifications of RSAE result from the advanced operation experiments in JT-60U [22] and JET [6]. Furthermore, the radial location of q_{min}, and consequently, of RSAE, is typically deep in the plasma core region, whereas TAE gener-

ally locates more externally with finite shear [40]. Thus, considering that the alpha particles are mostly generated in the plasma center, where the density and temperature profiles peak, the RSAE is expected to play a crucial role in nonlinear core SAW-EP dynamics of steady-state burning plasmas. In this review, after briefly analyzing the RSAE linear spectrum in typical burning plasma parameter regime using a simplified simulation model [40], we discuss several important issues in the nonlinear dynamics of RSAE. Namely, (i) the phase space structure of resonances between EP and RSAE, and the characteristics of EP self-consistent transport by RSAE [41, 42]. (ii) The coupling of multiple RSAEs and the nonlinear generation a generic low frequency Alfvénic mode (LFAM) [43]. The LFAM is a generalized terminology describing a rich spectrum of modes [16, 44] with predominant Alfvénic polarization [45] and $\omega \lesssim \omega_{\rm ti}, \omega_{*\rm pi}$, typically much lower than $\omega_{\rm A}$. Here, $\omega_{\rm ti} = v_{\rm i}/(qR_0)$ and $\omega_{*\rm pi} = (cT_{\rm i}/e_{\rm i}B_0^2)(\boldsymbol{k}\times\boldsymbol{B}_0)\cdot\nabla \ln P_{\rm i}$ are the thermal ion transit and diamagnetic drift frequencies, respectively, with $v_{\rm i} = \sqrt{2T_{\rm i}/m_{\rm i}}$ the ion thermal speed. Notable examples of LFAM include BAE, kinetic ballooning mode (KBM) [46], and Alfvénic ion temperature gradient (AITG) mode [47, 48] (see [49, 50] for recent theoretical analyses in reversed shear scenario). Since the LFAM could heat thermal ions via collisionless ion Landau damping, this novel spectral cascading mechanism may provide core-localized alpha channeling from EP to fuel ions, and thus, directly contribute to the enhancement of fusion performance. (iii) The spontaneous excitation of the axisymmetric zero frequency zonal field structures (ZFZSs) [51] by a finite amplitude RSAE via modulational instability [52]. This mechanism may have potential interest in not only the spectral energy transfer and the eventual saturation of the RSAE, but also in the core heat and particle transport, noting the important role of the ZS in regulating microscopic turbulences [53]. Of course, the above-listed topics within this brief review have no intention to be exhaustive, but rather to attract further research attentions on the unique role of the RSAE within the multi-scale dynamics of burning plasmas [2, 54].

The nonlinear physics through RSAE-EP resonant dynamics and the nonlinear wave-wave coupling will be elaborated in sections 2 and 3, respectively. Noting that SAW naturally exhibits two-scale mode structures along the extended poloidal angle [55] due to continuum coupling [12, 16, 46, 56], it is readily seen that the large orbit EP contribution mostly enters the ideal region, whilst the wave-wave coupling dominated by perpendicular scattering takes place in the singular inertial region [57, 58], where the thermal plasma contribution due to Reynolds (RS) and Maxwell (MX) stresses maximizes. This characterization also allows us to use different descriptions when focusing on different nonlinear physics. In section 2, we refer to a hybrid MHD-kinetic model [59], where the EP are treated kinetically and self-consistently coupled to the MHD equations which describe the RSAE fluctuations on mesoscopic spatiotemporal scales [2, 40, 54]. That is, the timescale under consideration is of the order of the inversed linear growth rate $1/\gamma_{\rm L}$ and the typical perpendicular wavelength of the mode envelope is comparable with the resonant EP orbits. More particularly, we rely on numerical simulations by the hybrid MHD-gyrokinetic code (HMGC) [60] using simplified but representative parameters. On the other hand, in section 3, the nonlinear gyrokinetic theory [61] is applied to properly capture the kinetic responses mandatory for perpendicular scattering [57], the wave-particle interaction important for collisionless fuel ion heating by the nonlinearly generated LFAM [43], as well as the trapped particle effects for neoclassical inertia enhancement crucial for ZFZS physics [51, 52, 62]. In section 3, in order to make analytical progress, the wave-EP resonance important for RSAE excitation is neglected; instead, we treat the RSAE as a prescribed finite amplitude pump wave, and focus on its nonlinear mode coupling processes [63]. Ultimately, a fully self-consistent description of the nonlinear wave-EP dynamics and quantitative assessment of the RSAE nonlinear saturation and EP transport must account for both nonlinear wave-wave coupling [43, 52, 64] and wave-particle interaction [40, 41] on the same footing, along with the multiple spatial and temporal scales that naturally appear [2, 54]. This is, however, very challenging via either analytical derivation or large scale numerical simulations, and beyond the scope of this brief review. Section 4 summarizes our present understandings and gives an outlook to possible future research topics.

2. RSAE-EP resonant dynamics

This section mostly focuses on the saturation process of the EP-driven modes due to wave-particle nonlinearity, that is, the modification of resonant particle trajectory by finite amplitude electromagnetic oscillations, which may lead to particle transport as well as self-consistent nonlinear evolution of the (typically single-n) wave, very often with the character of non-adiabatic frequency chirping [65–72]. As the resonant interaction between SAW and EP generally exhibits macro- or meso-scopic scales and depends sensitively on the detailed structures in the EP phase space, numerical simulations are generally needed. In addition, since we attempt to extract the generic characteristics of the RSAE saturation due to wave-particle nonlinearity, as well as the resultant EP transport, the simulations need to be sufficiently representative. Thus, we adopt a simplified simulation model with main parameters chosen to represent burning plasma conditions, which can be easily extrapolated to various devices, proposed or under construction, by means of a few dimensionless parameters [40, 41]. On the other hand, many machine-specific features are neglected, such as the plasma shaping and realistic particle distribution functions reflecting heating methods. Section 2.1 presents more details on the model assumptions and main parameters. As a necessary background to pave the way for the nonlinear analyses later on, we give an overview on the linear properties of the RSAEs in the simulations in section 2.2. Further-

more, the structures of RSAE-EP resonance in the phase space are analyzed in great detail; such an understanding could provide a direct implication on the nonlinear saturation mechanism and EP transport processes discussed in section 2.3.

2.1. Numerical model and parameters

The hybrid MHD-kinetic model [59], which is the foundation of many codes [60, 73–75], is a simple yet relevant model to study the nonlinear interactions between EP and MHD instabilities such as the SAW. In this model, the background plasma equilibrium and fluctuations are described by a set of MHD equations, whilst the EP are calculated kinetically, and couple with the MHD momentum equation through either the pressure or the current terms. Typically, a simulation case is initialized at an unstable condition with negligible perturbation amplitude, such that the most unstable mode driven by EP can be observed with a clear exponentially growing linear stage, followed by the eventual saturation due to nonlinear effects. Compared with a fully gyrokinetic approach as in section 3, the thermal plasma responses are simplified as a MHD model; however, the self-consistent wave-EP kinetic interactions are fully retained. That is, during both the linear growth and nonlinear evolution stages, the EP could impact or even significantly alter the MHD mode structures and real frequency, in addition to providing the driving mechanism of the mode spectrum; the EPM is a clear example [2, 12, 68, 76, 77]. This interaction is often referred to as the nonperturbative effect of the EP [12, 68], which has been shown to be important when comparing the measured and simulated RSAE mode structures in present-day devices [78], and is also expected to be significant for RSAEs in burning plasmas [40, 41].

The HMGC is utilized as the main research tool in this section. For simplicity, only the essential physics contents are described here; interest readers are referred to specific publications [60, 79, 80] for more details on the physics equations and the numerical treatments. In HMGC, the single-fluid MHD equations are in principle ideal [§], and are further reduced [81] by considering a large aspect ratio geometry with shifted circular cross sections, and neglecting the plasma compressibility. Thus, besides the effect of plasma shaping, which is less significant in the plasma core region, the coupling of RSAE with acoustic waves [82] is also neglected, and at the lowest order, the RSAE frequency follows that of the SAW continuum accumulation point (CAP), $\omega_A \simeq |nq_{\min} - m|v_A/(q_{\min}R_0)$. The scalar potential $\delta\phi$ and the parallel component of the vector potential $\delta A_\parallel$ are the two interconnected field variables. Furthermore, the MHD equations are linearized by evolving only a single toroidal mode number n in a simulation case, while nonlinear mode couplings are systematically neglected. In fact, the only retained nonlinear effect is the perturbation of the EP distribution function when the mode reaches a finite amplitude. Using particle-in-cell methods, the EP orbit is solved by a set of drift-kinetic equations [83] in HMGC. Thus, we neglect the FLR effect and but fully retain the finite drift orbit width (FOW) effect. The nonperturbative EP drive enters the MHD force balance equation via the divergence of the Chew-Goldberger-Low pressure tensor term [84].

The simulation parameters are mainly inferred from the proposed 'hybrid' operation scenario of the ITER [34], with weakly reversed magnetic shear in the core. Although it is our ultimate target to simulate the fully noninductive steady-state scenario of a fusion power plant, which typically has strongly reversed shear and elevated q profile under the present design [35, 38], there remain many open issues with this case such as balancing the current composition with plasma profiles and external power input. Meanwhile, the 'hybrid' scenario is much better understood and readily achievable in present and future devices, e.g., the Divertor Tokamak Test (DTT) facility currently under construction in Frascati, Italy [40, 41, 85]. Nominally, noting the large aspect ratio model of HMGC, we assume $R_0 = 10$ m, minor radius $a = 2$ m, on-axis magnetic field $B_{0,\text{axis}} = 5$ T. As RSAEs of interest here are typically core-localized, this large aspect ratio assumption will not significantly impact the results of the present analysis. Figure 2(a) shows the considered q profile, with $q_{\min} \simeq 1.028$ slightly above unity at about one third in the minor radius. Thermal ions are assumed to be deuterium with density $n_i = 2\times10^{20}$ m^{-3} and a flat radial profile for simplicity, as their gradient is not expected to be significantly impacting the RSAE spectrum in the core region. On the other hand, by neglecting the plasma compressibility and coupling with acoustic waves, the plasma temperatures are not explicitly considered here; $T_e = T_i = 20$ keV is assumed when evaluating the critical energy of the slowing-down EP distribution function [86].

As EP population, we consider only the fusion born alpha particles with birth energy $E_b = 3.52$ MeV, and use an isotropic slowing-down model. Figure 2(b) shows the assumed radial density profile with $n_{\text{EP,axis}}/n_i = 2\times10^{-3}$ and $\beta_{\text{EP,axis}} \simeq 0.63\%$. Note that similar pressure profile can be reproduced by a proper combination of multiple heating methods [87]. Finally, we note that all these nominal param-

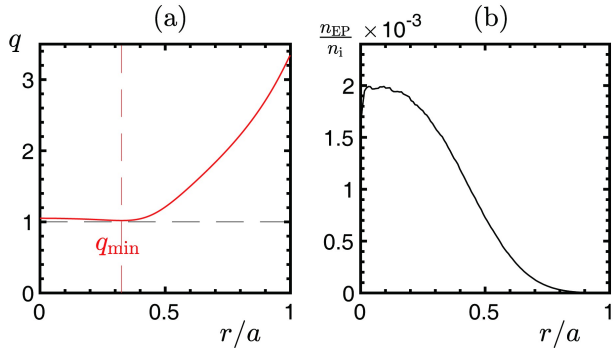

Figure 2. Equilibrium q profile (a) and EP density n_{EP} profile (b). The locations of $q_{\min}$ and $q = 1$ surfaces are indicated in (a).

[§]The derivation of model equations assumes ideal MHD condition, $\delta E_\parallel = 0$. However, as common in MHD codes, several small-valued numerical dissipation terms (mainly resistivity and viscosity) are still included, in order to dissipate the mode-converted radial singular structures [10] where the continuous spectrum is resonantly excited, and avoid grid-level numerical instability.

eters are assumed only to build a reasonable reference for these simulations, which could represent a generic burning plasma scenario [40]. In fact, besides the obvious factors like magnetic geometry and global profile nonuniformity, the SAW-EP dynamics can be reflected by a few dimensionless parameters. Among them, we emphasize the characteristic speed ratio $v_{\rm EP}/v_{\rm A,axis} \equiv \sqrt{E_{\rm b}/m_{\rm EP}}/v_{\rm A,axis} \simeq 1.684$, which dictates the resonance condition; and the normalized EP Larmor orbit width $\rho_{\rm EP}/a \equiv v_{\rm EP}/(\omega_{\rm c,EP,axis}a) \simeq 0.0192$, which is considerably smaller than present day devices, and connects with the most unstable mode due to the important role of orbit averaging in determining the drive intensity (see section 2.2).

2.2. Linear properties and the resonance condition

We begin this section by inspecting the RSAE linear spectra in multiple simulation cases with different n. Figure 3 overviews the modes' radial structures and spectra as functions of n in the range of $n = 3-17$, and as a reference case with $n = 10$, figure 4 gives an example of the RSAE mode structures. For lower $n = 1$ and 2, the modes behave like fishbones [88] and are not of our interest here. At higher $n \geq 16$ with the RSAE frequency approaching the TAE gap for the present equilibrium with $q_{\rm min} \simeq 1.028$, the TAEs localized nearby the $q_{\rm min}$ surface are also unstable, and merge with the RSAE branch at $n = 18$ with $k_{\parallel}q_{\rm min}R_0 \simeq 1/2$. Note that in the present simulations, by considering $q_{\rm min}$ marginally above an integer, the RSAE frequency lies close to the minimum point of the continuum [24], and has a nearly linear dependence with n, as can be seen from figure 3 (a), where the modes with adjacent n are almost equidistant in frequency space. These RSAEs, although generally rare in present day devices, could still be excited if such an equilibrium can be maintained to avoid strong sawtooth events, and are shown to have quite similar properties to the more common RSAEs above the local continuum maximum point with $q_{\rm min}$ slightly below a rational value [30, 31, 89, 90]. Meanwhile, the linear growth rate $\gamma_{\rm L}$ versus n in figure 3(b), shows that $\gamma_{\rm L}$ first gradually increases with n, then becomes nearly invariable at around $n \simeq 10$, before a second increase appears at higher n. The underlying reason for the variation of $\gamma_{\rm L}$, i.e., the linearly most unstable mode, is associated with different driving source in the EP phase space as well as the orbit averaging effect for the drive intensity [40]. By inspecting the phase space power transfer diagram in the EP phase space [91], it is found that at lower n ($n \lesssim 10$), the RSAEs near the BAE frequency range are almost purely driven by the magnetically trapped EP via the precession resonance [76]. With increasing n and thus ω, the transit resonance with mostly barely counter-circulating EP also becomes appreciable and gradually dominant. The location of significant resonant drive in the velocity space is shown in figure 5(a) for $n = 10$ in the transition between the two regimes. On the other hand, the variation of $\gamma_{\rm L}$ within each regime can be understood from the maximized EP drive intensity condition as $k_{\perp}\rho_{\rm d,EP} \sim O(1)$ [12, 18, 93], with $\rho_{\rm d,EP}$ the drift orbit width of EP in the present model. In more details, noting that the EP drive intensity scales with its diamagnetic frequency $\omega_{*,\rm EP} \propto m$ [94, 95], higher-n modes would receive stronger drive without considering other effects. Meanwhile, the perpendicular wavenumber $k_{\perp}$ dominated by $k_{\theta} \propto m$ also increases with n, and when the wavelength $1/k_{\perp}$ becomes comparable with the EP orbit width, orbit averaging effect kicks in and limits the most unstable mode number with $k_{\perp}\rho_{\rm d,EP} \sim O(1)$. Indeed, as can be estimated from the poloidal mode structure and resonant EP's

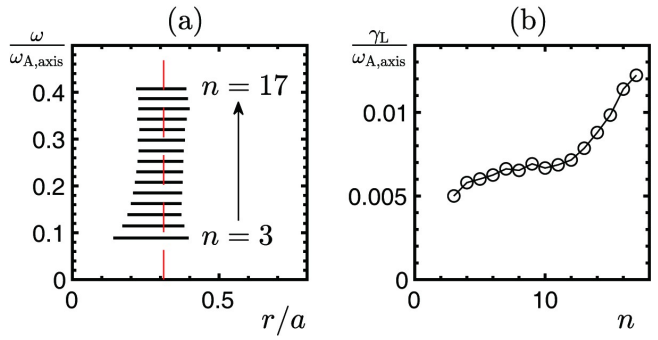

Figure 3. (a) The frequencies and radial locations for the RSAEs in the simulations, where each segment indicates the radial range with amplitude larger than 10% of the peak amplitude. (b) The linear growth rate $\gamma_{\rm L}$ versus n.

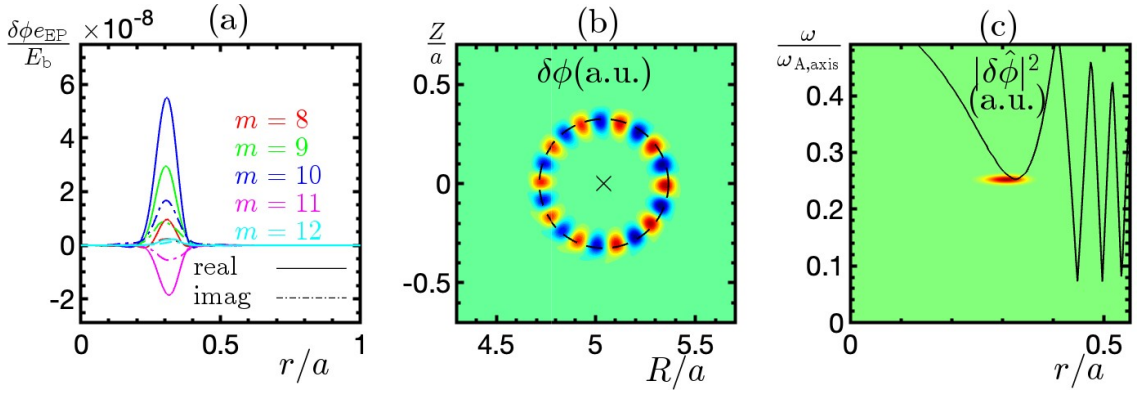

Figure 4. For the $n = 10$ RSAE in the linear stage, (a) fourier decomposed radial structure of $\delta\phi$; (b) in the poloidal plane, where the magnetic axis and the $q_{\rm min}$ flux surface are indicated; (c) frequency spectrum $\hat{\delta\phi}^2(r,\omega)$ by fast Fourier transform in time and integration in poloidal angle, the solid curve is the theoretically calculated SAW continuum.

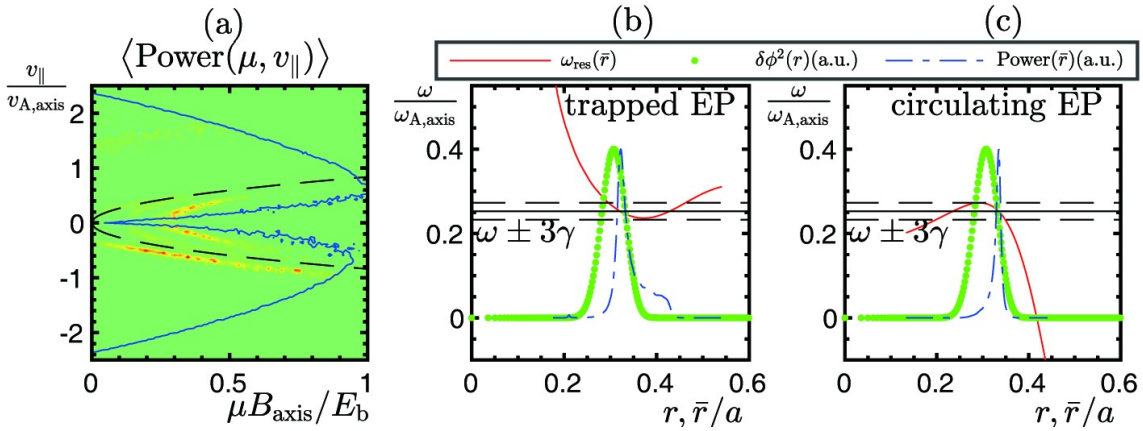

Figure 5. For the $n = 10$ RSAE in the linear stage, (a) volume averaged wave-EP power transfer intensity in the $(\mu, v_\parallel)$ space, positive data (red-yellow) denotes drive. The blue curve roughly indicates the boundary of the EP distribution function (contour line of 5% of the peak value), the black dashed parabola is the theoretically estimated trapped-circulating boundary [92] at q_{min}. Radial resonance structures from trapped (b) and circulating (c) test particle samples, including the resonance frequency $\omega_{res}(\bar{r})$ (red curve) with $\bar{r}$ the orbit averaged radius of the particle, the radial mode structure $\delta\phi^2(r)$ (green dots), and the power transfer profile by the test particle sample (blue, dash-dotted curve). The horizontal lines indicate the range of mode frequency for effective resonant interaction (ω and $\omega \pm 3\gamma$).

drift orbit [40], at $n \simeq 10$, $k_\perp \rho_b \simeq 1.2$ for the banana orbit of trapped EP, corresponding to the first peak in figure 3(b) around $n \simeq 10$. Meanwhile, $k_\perp \rho_t \simeq 0.3$ at $n \simeq 10$ for the transit orbit of circulating EP, noting that $\rho_t \sim \epsilon^{1/2}\rho_b$ with $\epsilon = r/R$ the inverse aspect ratio, and thus, the most unstable mode number dominated by circulating EP resonance is expected to be around $n \sim 20-30$. In any case, one could reasonably conclude that the most unstable mode number for RSAE in the present burning plasma scenario is $n \sim O(10)$, implying that the SAW-EP dynamics indeed takes place on the mesoscale. Similar linear studies generally give the most unstable mode numbers in the range of $n \sim 20-30$ for core-localized TAEs with weak shear driven by circulating alpha particles in ITER-like burning plasmas [96–100], consistent with the trend in figure 3(b) and the argument given here.

We then investigate the structure of the RSAE-EP resonance in the phase space by following the orbits of a characteristic set of resonant particle sample as test particles. In accordance with the nonlinear investigations in the next section 2.3, these test particles are chosen to have the same constants of motion in the presence of perturbations; namely, the magnetic moment μ and the extended Hamiltonian $E' \equiv E - \omega P_\varphi/n$ [101]. Here, P_φ is the canonical toroidal angular momentum, which is a constant of motion without perturbations, and its value roughly represents the opposite of the poloidal magnetic flux, representing the radial flux coordinate. Due to the conservation property of μ and E', at the lowest order, such a phase space sample is preserved through the nonlinear phase, and thus, is suited for an isolated examination of the resonant EP dynamics [91, 102]. As suggested by figure 5(a), we choose samples from both trapped and circulating regions, with $\mu B_{axis}/E_b = 0.4$, $E'/E_b = 0.396$ for the trapped sample, and $\mu B_{axis}/E_b = 0.3$, $E'/E_b = 0.354$ for the counter-circulating one; and both sets of test particles are distributed around the radial range of the mode location. The resonance structures in the radial space are shown in figures 5(b) and (c), where the orbit averaged radial coordinate $\bar{r}$ of the test particle is used for a better comparison with the radial mode structure. Note that the relevant resonance frequency ω_{res} depends on the particle's orbit type and resonance mechanism. For the magnetically trapped particles (figure 5(b)), the dominant resonance is the bounce-averaged toroidal precession drift,

$$\omega_{res} = n\overline{\omega_d}, \tag{1}$$

while for circulating particles (figure 5(c)), the transit resonance takes the form [68]

$$\omega_{res} = n\overline{\omega_d} + (n\bar{q} - m + p)\omega_t, \tag{2}$$

with the drift frequency $\overline{\omega_d}$ typically much smaller than the transit frequency $\omega_t \simeq v_\parallel/qR$ for well circulating particles, $\bar{q}$ is the orbit averaged value of q, and p is an integer corresponding to the considered harmonic in the drift orbit expansion. In figure 5(b), one sees that for the deeply trapped EP, $\overline{\omega_d}$ essentially scales as $1/r$ radially [76]. Thus, apart from the region very close to the magnetic axis, ω_{res} is not significantly varying radially, and is close to the mode frequency in a quite broad radial domain, as can be also confirmed by the radial profile of power transfer by the test particle sample, whose radial width is comparable with the one of the mode. In fact, figure 5(b) shows some finite mode drive in the radial layer $\bar{r}/a \sim 0.38-0.43$ outside of the radial mode location $\delta\phi^2(r)$, due to the fact that these resonant EP's fat banana orbit only partly overlaps with the RSAE. As a result, the effective range of $\bar{r}$ (the bounce averaged particle guiding center position) for wave-particle power exchange can be broadened with respect to the mode structure by a length of the order of the resonant particle radial orbit width (see Appendix A of [68] for further details). All together, this evidence indicates that the radial range where resonant wave-EP interaction could take place is clearly limited by the finite radial range of the localized RSAE mode structure, rather than the resonance condition $\omega_{res} \simeq \omega$. In figure 5(c), we also find a quite similar resonance structure near the RSAE radial location for the circulating EP. If one neglects

the first term on the right hand side (RHS) of equation (2), it can be easily found that $\partial_r\omega_{\rm res}$ is mostly determined by $\partial_r\bar{q}$, i.e., the magnetic shear, which always vanishes around the radial location of RSAE. Thus, a relatively flat $\omega_{\rm res}(r)$ profile, and correspondingly, a radially resonant region comparable with the mode width, is also expected for the circulating EP [42]. In contrast, as shown in [41], the resonance structure of circulating EP would be significantly different for the outer-core TAEs with finite magnetic shear. The much greater $\partial_r\omega_{\rm res}$ induces radially very narrow resonant region and sharp peaks in the power transfer profile, and potentially leads to different saturation mechanism [41, 68]. Compared with the TAE, the radially broad resonance structure of the RSAE is due to its high mode number and lower frequency, such that the precession resonance with trapped EP is possible, and also due to the weak/vanishing magnetic shear near the mode location when resonating with circulating EP. Nonlinearly, such resonance structures suggest that the resonant EP's response to the mode would be nonlocal, due to the fact that the resonant EP could explore the whole radially nonuniform mode structure during radial transport, as allowed by the resonance condition [41, 68, 91, 102, 103].

2.3. Nonlinear saturation and EP transport

In this section, we only focus on the saturation process due to the self-consistent wave-EP nonlinear dynamics. That is, with increasing RSAE amplitude and resonant EP orbit excursion, the EP drive intensity associated with phase space gradient is gradually weakened, and the saturation is reached when the drive eventually drops to the level of the background damping which is induced by the resistive-like terms in the present MHD model, as shown in figure 6(a) for the time evolution of the peak value of $\delta\phi$. This nonlinear process takes place on very short timescales, $O(1/\gamma_{\rm L})$ [68]. On the other hand, the nonlinear saturation to be analyzed in section 3 generally assumes such a finite amplitude RSAE as the initial condition, and focuses on its nonlinear coupling with other waves on typically much longer timescales. The eventual saturation amplitude obtained therein may provide a more comprehensive indication of the RSAE's impact to fusion performance.

As anticipated above, the analyses on the radial structure of RSAE-EP resonance bear significant implications to the mechanisms of RSAE's nonlinear saturation and EP transport [41, 91, 102, 103]. To see this more in detail, we again utilize the isolated resonant test particle sample shown in figures 5(b) and (c). An efficient way to visualize the transport process is to map the particles' canonical coordinates into a series of Poincaré frames [104] and observe the change of phase space topology. Figures 6(b)–(d) show several time frames in the (Θ, P_φ) plane for the trapped EP sample in figure 5(b), where $\Theta = -\omega t + n\varphi$ is the relative

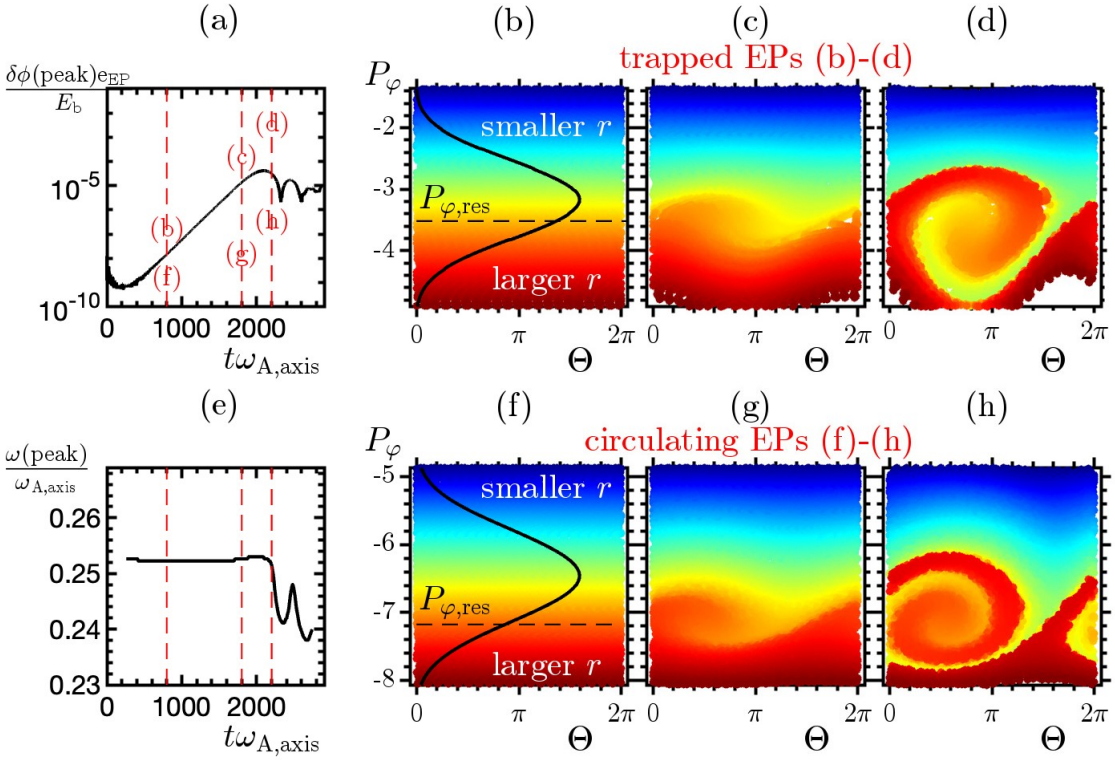

Figure 6. (a) Time evolution of the peak value of $\delta\phi$. Red dashed vertical lines indicate the time of the phase space snapshots of following figures. (b)–(d) Poincaré plots in the (Θ, P_φ) plane of the trapped test particle sample at three different times. Here, P_φ is normalized by $m_{\rm EP}av_{\rm A,axis}$. The particle markers are colored by its initial value of P_φ, the location of $P_{\varphi,\rm res}$ where $\dot{\Theta}=0$ in the linear stage is indicated by a horizontal dashed line. The radial mode structure $\delta\phi^2(r)$ is plotted in (b) by mapping $r\mapsto\bar{r}$ and then to P_φ coordinate in the linear stage. (e) Time evolution of the mode frequency at the peak value of the integrated frequency spectrum $\delta\hat{\phi}^2(r,\omega,t)$. (f)–(h) Same as (b)–(d) for the circulating test particle sample.

wave-particle phase evaluated at $\theta = 0$; and figures 6(f)–(g) for the circulating particle sample. Here, in order to give an indication of the corresponding radial range, the linear radial mode structures $\delta\phi^2(r)$ are mapped into P_φ coordinate via the $\bar{r}$ of the test particles in the linear stage. Taking the trapped EP as an example, in the linear stage with negligible RSAE amplitude (figure 6(b)), P_φ remains conserved, and the particle markers are streaming along the horizontal axis with shifting phase. The direction and speed of this streaming are determined by the minute difference of $\omega_{\rm res}$ and ω shown in figure 5(b), and one has $\dot{\Theta} = 0$ where $\omega_{\rm res}(P_{\varphi,\rm res}) = \omega$, as indicated by a horizontal dashed line in figure 6(b). Utilizing this property, in figure 6, all particle markers are colored (from blue to red) by its initial value of P_φ throughout the nonlinear evolution, such that the nonlinear variation of P_φ, i.e., phase space transport, would become evident. Indeed, when the RSAE amplitude grows to finite (figure 6(c)), the conservation property of P_φ breaks down, one sees that the colored markers start to cross the $P_{\varphi,\rm res}$ line. Note that, during this stage, since figure 5(b) shows that the resonance condition remains nearly satisfied in the radial domain of the mode location, Θ keeps quasi-stationary and the transported EP retain a coherent bundle. With $\dot{\Theta} \simeq 0$, the resonance condition is substantially maintained, and the transported EP keep driving the mode, as can be seen from figure 6(a) that the growth rate remains nearly unweakened in this stage. This phenomenon, dubbed 'phase locking', was first shown when simulating the trapped EP transport induced by $n = 1$ fishbones [105], and indicates that the EP transport here has a convective nature [77, 106]. The main difference with respect to the global fishbone is the radially localized mode structures for the $n \sim O(10)$ RSAEs. Indeed, the transport weakens when the resonant EP reach the radial boundary of the mode location, i.e., radially decouple with the mode, phase slips by roughly π, and these EP stream back in phase. At the timing of mode saturation, figure 6(d) shows the formation of a phase space resonance island, whose radial range is clearly comparable with, and in fact, limited by the finite scale of the radially localized RSAE mode structure. Thus, the predominant saturation mechanism for the RSAE here is the 'radial decoupling', rather than the 'resonance detuning' [2, 68]. Note that the 'resonance detuning' mechanism is expected to play important roles at marginal stability [107]. Nevertheless, as shown in the EP density scan in [41], the 'radial decoupling' mechanism, and the accompanied convective EP transport, are significant for RSAEs even with sufficiently weak drive, whilst the outer-core TAEs are dominated by 'resonance detuning' at similar growth rates. As mentioned above, all these features can be traced back to the peculiar phase space resonance structure for the RSAE in figure 5(b), and also apply to the circulating EP with the similar radial resonance structures (figure 5(c)), as shown in figures 6(f)–(h) for completeness.

The simulation finding follows from the unified theoretical paradigm of EP transport in burning plasmas [2, 68, 69, 108], and, when applied to a single-n RSAE predominantly driven by an isolated resonance, it suggests that a core-localized RSAE would generally induce coherent and convective EP phase space flows in the radial range of the mode location. The EP transport includes both radially inward and outward particle flows; however, the net effect is an outward particle flux due to the nonuniform EP distribution function. This agrees remarkably well with the recent observations in DIII-D, in which quite a large scale EP phase space flux is possibly induced by the global mode structures of low-n RSAEs [109]. Based on the simplified simulations here and envisioning the much more complex burning plasmas, two possible consequences are predicted theoretically, depending on the EP-drive intensity and the number of modes involved. If the EP are strongly driving the RSAE and show significant nonperturbative effect, i.e., the RSAE has clear EPM features to maximize the resonant EP drive, the mode structure and frequency would also undergo significant modification following the self-consistent evolution with the EP transport [41, 42]. A typical signature is the fast, nonadiabatic frequency chirping of the RSAE [41, 42, 77], in addition to its usual frequency sweeping behavior due to equilibrium evolution in much longer timescales [110–112]. In fact, the nonadiabatic frequency chirping is already evident in the present simulations, as can be seen in figure 6(e) that the peak frequency of the wave packet is oscillating with the same frequency of the mode amplitude pulsation, which is of the order of the typical resonant EP 'bounce' frequency $\omega_{\rm B}$ inside the phase space resonance island of figures 6(d) and (h) [2, 68]. The details of the nonadiabatic frequency chirping of EP-driven SAW is beyond the scope of the present review, and readers are referred to more specific publications on the recent advancement in understanding the underlying physics in various physics contexts [42, 113, 114]. Here, we only note that one possible wave branch may undergo convective amplification by continuing to maintain the resonance condition with the EP and following the convective EP flux; the radially propagating wave packet would bring forward more resonant particles by shifting the resonant region in phase space [7, 68, 72, 77]. This is severely dangerous for EP confinement since it may break good Kolmogorov-Arnold-Moser (KAM) surfaces and lead to avalanche-like global EP transport [98, 115, 116]. Another scenario is when the system contains a large number of low amplitude modes [3], which may be more likely in steady-state burning plasmas since a broad spectrum of RSAEs may be simultaneously unstable, as suggested by the linear analysis in section 2.2. The phase space resonance islands of EP with different modes could easily overlap and decorrelate the coherent phase space structures. In this case, the EP transport may also exhibit a random-walk-like diffusive character [117, 118]. The role of convective versus diffusive EP transport induced by RSAEs in the core of burning plasmas, of course, depends on the considered scenario, and both mechanisms might even coexist when inspecting different scales. This is a subject of on-going researches and will be reported in future publications. Nevertheless, we note that either of these transport mechanisms could lead to nonlocal

EP transport and probably connects with the outer-core modes such as the TAE. In this regard, a key parameter in burning plasma operation may be played by the radial location of the $q_{\min}$ surfaces, which relates with the closeness of phase space resonances between core-localized RSAEs and outer-core TAEs. Previous numerical works on the ITER hybrid scenario suggest that an EP transport barrier between core-localized and outer-core TAEs may exist with minimal local diffusion [100]; however, a domino-like effect leading to successive global EP transport is also possible [98]. Overall, a thorough characterization of the RSAEs' impact to EP confinement is nontrivial and requires both large scale global simulations and advanced transport models. Here, it is worthwhile to note that a systematic theoretical formalism for analyzing wave-particle interactions and the ensuing self-consistent EP transport has been developed based on the description of renormalized nonlinear neighbouring equilibria varying on the mesoscales and the long-lived phase space zonal structure (PSZS) evolution [2, 68, 69, 108, 119]. This understanding provides us a possible framework to calculate the long timescale SAW-EP nonlinear interplay in realistic geometry with affordable computational demands, and is actively pursued envisioning the burning plasma operation in the near future.

3. Nonlinear wave-wave couplings

In the previous section 2, it has been shown that a broad spectrum of RSAEs could be readily excited by EP in the core of a burning plasma, and may reach appreciable amplitudes. Naturally, their further nonlinear evolutions become the next question. As shown in [58] by simply manipulating the ideal MHD momentum equation in a uniform plasma, a large amplitude SAW could exist due to the exact cancellation of the nonlinear terms, namely, the Reynolds and Maxwell stresses. Meanwhile, various nonideal effects, notably the magnetic geometry, plasma nonuniformity, compressibility and kinetic effects, could break such a 'pure Alfvénic state' [1] and lead to nonlinear spectral energy transfer by coupling with other collective oscillations [2, 58, 63]. These nonideal effects, which must be accounted for when studying SAW instability nonlinear dynamics and EP transport in burning plasmas, have been intensively investigated using TAE as a paradigm case [51, 120–127], as recently reviewed in [128]. The developed theoretical framework and obtained insights can be straightforwardly applied to other kinds of SAW instabilities, e.g., RSAE, which is the subject of this section, based on the understanding of RSAE linear physics and saturation due to wave-particle interactions as reviewed in section 2.

Note that when the kinetic responses of thermal plasmas in the short wavelength regime that dominate the inertial layer contribution to RS&MX are considered, the core plasma fluid description as in section 2 is generally insufficient, and the nonlinear gyrokinetic theory [61] must be adopted to properly account for key physics such as the trapped particle contribution to neoclassical inertial enhancement crucial for zero frequency zonal flow [58, 62]. A demonstration for the necessity of the nonlinear gyrokinetic approach is the paradigm case of the nonlinear parametric decay of a pump KAW into an ion sound wave and a KAW sideband [11, 57], where it is shown that not only the nonlinear drive is quantitatively enhanced compared to the MHD regime [63], but also the scattering cross section is qualitatively changed, with significant implication to plasma transport. The theoretical framework and the governing equations are elaborated in section 3.1, based on which, in the following sections, we derive the dispersion relations of two important nonlinear wave-wave coupling channels for the RSAE nonlinear evolution [43, 52], identify the parameter regimes for them to occur, and estimate the threshold conditions of their onset. To make analytical progress, we also treat this coupled system as a long timescale saturation problem by looking for fixed point solutions [129], which may shed light on the RSAEs' impact to fusion performance.

In principle, there could be many possible channels for wave-wave coupling as either spontaneous decay or forced driven processes, due to the rich electromagnetic oscillations in plasmas with dominant collective behaviors as a result of the long-range electromagnetic forces. Thus, the examples shown in this section are necessarily simplified and selected based on their potential important role in the RSAE nonlinear dynamics and fusion performance. As many RSAEs as well as their kinetic counter-part [18], the KRSAEs, exist with radially overlapped mode structures and generally separated frequencies (see figure 3(a)), they may naturally couple and possibly excite a LFAM as suggested by their small frequency differences. In section 3.2, we present a general paradigm of three SAWs coupling in the nonlinear gyrokinetic regime, and apply to the scenario of a pump RSAE decaying into another RSAE and a LFAM. Besides determining the RSAE nonlinear saturation spectrum and EP transport, this process may have potential roles on the collisionless heating of fuel ions by the LFAM Landau damping. On the other hand, a finite amplitude SAW with a coherent radial envelope could become modulationally unstable, and spontaneously excite the toroidally symmetric ZFZS [51]. The dispersion relation of the modulational instability and the impact to RSAE saturation are discussed in section 3.3.

3.1. Theoretical model

For simplicity and clarity, similar to section 2, we also take a large aspect ratio tokamak equilibrium with shifted circular magnetic surfaces. The electromagnetic fields are described by $\delta\phi$ and $\delta A_\parallel$. Here, $\delta B_\parallel$ is consistently neglected as plasma $\beta \ll 1$, but finite $\delta E_\parallel$ and kinetic compressibility are fully retained. For convenience, we take $\delta\psi \equiv \omega\delta A_\parallel/(ck_\parallel)$ as alternative variable for the induced field, such that $\delta E_\parallel = 0$ corresponds to $\delta\phi = \delta\psi$.

The governing equations describing nonlinear interactions of three waves coupling include the nonlinear gyroki-

netic vorticity equation derived from the parallel Ampère's law, quasi-neutrality condition and nonlinear gyrokinetic equation [2, 130, 131]. The first two equations read

$$\frac{c^2}{4\pi\omega_k^2}B\frac{\partial}{\partial l}\frac{k_\perp^2}{B}\frac{\partial}{\partial l}\delta\psi_k+\frac{e^2}{T_\mathrm{i}}\left\langle\left(1-J_k^2\right)F_0\right\rangle\delta\phi_k-\sum_{s=\mathrm{e,i}}\left\langle\frac{q}{\omega_k}J_k\omega_\mathrm{d}\delta H_k\right\rangle_s$$
$$=-\frac{\mathrm{i}}{\omega_k}\sum_{\boldsymbol{k}=\boldsymbol{k}'+\boldsymbol{k}''}\Lambda^{\boldsymbol{k}}_{\boldsymbol{k}'',\boldsymbol{k}'}\left[\frac{c^2}{4\pi}k_\perp''^2\frac{\partial_l\delta\psi_{k'}\partial_l\delta\psi_{k''}}{\omega_{k'}\omega_{k''}}\right.$$
$$\left.+\left\langle e\left(J_kJ_{k'}-J_{k''}\right)\delta L_{k'}\delta H_{k''}\right\rangle\right], \tag{3}$$

$$\frac{n_0e^2}{T_\mathrm{i}}\left(1+\frac{T_\mathrm{i}}{T_\mathrm{e}}\right)\delta\phi_k=\sum_{s=\mathrm{e,i}}\left\langle eJ_k\delta H_k\right\rangle_s. \tag{4}$$

Noting that $k_\perp\rho_{\mathrm{d,EP}}\sim O(1)$ for the pump RSAE, and thus, $k_\perp\rho_\mathrm{i}\ll 1$, the quasi-neutrality condition (4) can be sometimes simplified as the nonlinear ideal Ohm's law,

$$\delta E_{\parallel,k}=-\sum_{\boldsymbol{k}=\boldsymbol{k}'+\boldsymbol{k}''}\boldsymbol{b}\cdot\delta\boldsymbol{u}_{k'}\times\delta\boldsymbol{B}_{k''}/c, \tag{5}$$

with $\delta\boldsymbol{u}$ being the $\boldsymbol{E}\times\boldsymbol{B}$ drift velocity. Here, the three terms on the left hand side (LHS) of the vorticity equation (3) denote the field line bending, inertia, and the curvature coupling, respectively. The two terms on the RHS are formally nonlinear and correspond to MX and RS, respectively [131]. ∂_l is the derivative along the direction of the equilibrium magnetic field $\boldsymbol{b}\equiv\boldsymbol{B}_0/B_0$; $J_k\equiv J_0(k_\perp\rho)$ is zeroth order Bessel function accounting for the FLR effect; $\omega_\mathrm{d}=(v_\perp^2+2v_\parallel^2)(2\Omega_\mathrm{c}R_0)(k_r\sin\theta+k_\theta\cos\theta)$ is the magnetic drift frequency; $\langle\ldots\rangle$ denotes velocity space integration; $\Lambda^{\boldsymbol{k}}_{\boldsymbol{k}'',\boldsymbol{k}'}=(c/B_0)\boldsymbol{b}\cdot\boldsymbol{k}''\times\boldsymbol{k}'$ accounts for the perpendicular scattering; and $\delta L_k\equiv\delta\phi_k-k_\parallel v_\parallel\delta\psi_k/\omega_k$.

Here, as noted above, we assume the nonlinear evolution of the pump RSAE with a prescribed amplitude, while neglecting its linear excitation by EP, due to their typically negligible contribution to RS&MX in the fast varying inertial layer where $k_\perp\rho_\mathrm{EP}\gg 1$ [16, 46]. Instead, the nonlinear mode coupling is dominated by thermal plasmas [51, 57], which are consistently described by the nonlinear gyrokinetic approach. The nonadiabatic particle responses δH_k for electron/ion species (subscript 's', which is suppressed when possible), contained in the perturbed distribution function,

$$\delta f_k=-\left(\frac{e}{T}\right)_s F_0\delta\phi_k+\mathrm{e}^{-\rho\cdot\nabla}\delta H_k,$$

are solved from the nonlinear gyrokinetic equation [61]

$$\left(-\mathrm{i}\omega_k+v_\parallel\partial_l+\mathrm{i}\omega_\mathrm{d}\right)\delta H_k=-\mathrm{i}\omega_k\left(\frac{e}{T}\right)_s F_0J_k\delta L_k$$
$$-\sum_{\boldsymbol{k}=\boldsymbol{k}'+\boldsymbol{k}''}\Lambda^{\boldsymbol{k}}_{\boldsymbol{k}'',\boldsymbol{k}'}J_{k'}\delta L_{k'}\delta H_{k''}. \tag{6}$$

The equilibrium distribution function F_0 is assumed to be Maxwellian, and again, in equation (6), effects associated with plasma profile nonuniformity are neglected, since diamagnetic frequencies of the core plasma are small compared with the RSAE frequency in the wavelength regime of interest here.

3.2. Parametric decay of RSAE and LFAM excitation

The first nonlinear mode coupling of RSAE presented, is the direct coupling among multiple unstable/stable RSAEs and/or their kinetic counterpart, KRSAEs, and the nonlinear excitation of secondary SAW modes. This is possible since there are many RSAEs simultaneously excited with radially overlapped structures in the reversed-q region, forming a rich and broad spectrum. As the RSAEs/KRSAEs satisfy, $\omega^2\simeq k_\parallel^2v_\mathrm{A}^2$ to the lowest order, when they couple, the generated modes will naturally satisfy the SAW dispersion relation. Among them, the lower frequency Alfvénic mode induced by two counter-propagating RSAEs/KRSAEs may resonantly interact with thermal ions, leading to collisionless fuel ion heating, and is of particular interest for future reactors.

As all three modes involved are SAWs, we first consider a generic scenario of three modes coupling with predominant SAW polarization, and then apply to the specific case of LFAM spontaneously excited by a pump RSAE. For simplicity of the derivation, we consider the 'local' limit and neglect the effect of plasma nonuniformity, corresponding to the limit that $\omega_{*\mathrm{pi}}$ is much smaller than the LFAM frequency. Thus, the present formalism applies to BAE as LFAM branch straightforwardly, but should be properly extended to account for the diamagnetic effect [132] when considering KBM or AITG.

To begin with, we note the ordering $|k_\parallel v_\mathrm{e}|\gg\omega\gg|k_\parallel v_\mathrm{i}|,\omega_\mathrm{d}$, and one has the linear particle responses $\delta H^{(0)}_{\mathrm{i},k}=eF_0J_k\delta\phi_k^{(0)}/T_\mathrm{i}$ and $\delta H^{(0)}_{\mathrm{e},k}=-eF_0J_k\delta\psi_k^{(0)}/T_\mathrm{e}$ at the leading order. Substituting into the quasi-neutrality equation (4), it shows that the ideal MHD condition $\delta\phi_k^{(0)}\simeq\delta\psi_k^{(0)}$ is maintained at the leading order, while it breaks down at the next order due to ion compressibility [57]. Meanwhile, from the vorticity equation (3) one derives the SAW dispersion relation

$$\frac{n_\mathrm{i}e^2}{T_\mathrm{i}}b_k\mathcal{E}_k\delta\phi_k^{(0)}=0. \tag{7}$$

Here, $b_k\equiv k_\perp^2\rho_\mathrm{i}^2/2$,

$$\mathcal{E}_k\simeq 1-k_\parallel^2v_\mathrm{A}^2/\omega_k^2-\omega_\mathrm{G}^2/\omega_k^2, \tag{8}$$

is the SAW dielectric function in the local WKB limit, with $\tau\equiv T_\mathrm{e}/T_\mathrm{i}$ and $\omega_\mathrm{G}=\sqrt{7/4+\tau}(v_\mathrm{i}/R_0)$ the leading order geodesic acoustic mode (GAM) frequency [133–136] that accounts for the SAW continuum upshift and the creation of the beta-induced SAW continuum gap [16]. Note that $\mathcal{E}_k$ here does not contain the effect of wave-particle resonances, consistent with the frequency ordering above. However, the anti-Hermitian part will be formally reinstalled [16] when considering the thermal plasma heating via the LFAM ion Landau damping below.

Considering $\boldsymbol{\Omega}_k(\omega_k,\boldsymbol{k})$ generated by the coupling of $\boldsymbol{\Omega}_{k'}(\omega_{k'},\boldsymbol{k}')$ and $\boldsymbol{\Omega}_{k''}(\omega_{k''},\boldsymbol{k}'')$, and noting the leading order particle responses, one has

$$b_k\left(-\frac{k_\parallel^2 v_{\rm A}^2}{\omega_k^2}\delta\psi_k+\delta\phi_k-\frac{\omega_{\rm G}^2}{\omega_k^2}\right) \simeq -\frac{\mathrm{i}}{\omega_k}\Lambda^{\boldsymbol{k}}_{\boldsymbol{k}'',\boldsymbol{k}'}\left(b_{k''}-b_{k'}\right)\left(1-\frac{k'_\parallel k''_\parallel v_{\rm A}^2}{\omega_{k'}\omega_{k''}}\right)\delta\phi_{k'}\delta\phi_{k''}, \tag{9}$$

from equation (3), and

$$\delta\phi_k-\delta\psi_k\simeq-\frac{\mathrm{i}}{k_\parallel}\Lambda^{\boldsymbol{k}}_{\boldsymbol{k}'',\boldsymbol{k}'}\left(\frac{k'_\parallel}{\omega_{k'}}-\frac{k''_\parallel}{\omega_{k''}}\right)\delta\phi_{k'}\delta\phi_{k''}, \tag{10}$$

from equation (5). Combining equations (9) and (10), one obtains

$$b_k\mathcal{E}_k\delta\phi_k=-\frac{\mathrm{i}}{\omega_k}\Lambda^{\boldsymbol{k}}_{\boldsymbol{k}'',\boldsymbol{k}'}\alpha^{\boldsymbol{k}}_{\boldsymbol{k}'',\boldsymbol{k}'}\delta\phi_{k'}\delta\phi_{k''}, \tag{11}$$

describing the evolution of $\boldsymbol{\Omega}_k$ due to the nonlinear beating of $\boldsymbol{\Omega}_{k'}$ and $\boldsymbol{\Omega}_{k''}$, with

$$\alpha^{\boldsymbol{k}}_{\boldsymbol{k}'',\boldsymbol{k}'}=\left(b_{k''}-b_{k'}\right)\left(1-\frac{k'_\parallel k''_\parallel v_{\rm A}^2}{\omega_{k'}\omega_{k''}}\right)+b_k v_{\rm A}^2\frac{k_\parallel}{\omega_k}\left(\frac{k'_\parallel}{\omega_{k'}}-\frac{k''_\parallel}{\omega_{k''}}\right), \tag{12}$$

the nonlinear coupling coefficient. The first term on the RHS of equation (12) is due to the competition of MX and RS, and the second one is the finite $E_\parallel$ term arising from the field line bending term.

Despite its simple form, equation (11) describes rich phenomenology. Two types of scenarios can be distinguished, namely, a spontaneous decay process where an unstable SAW decays to other two stable SAWs; and a forced driven process as two finite amplitude SAWs beat to a third one. For example, considering the high frequency range with $\omega\gg\omega_{\rm G}$ and all three SAWs are normal modes satisfying $\omega\simeq k_\parallel v_{\rm A}$, the frequency matching conditions can be naturally satisfied. E.g., equation (11) can be applied for the coupling among TAE, ellipticity induced AE and noncircular triangularity induced AE [127]. If the parallel electric field due to kinetic effect is properly considered [57], equation (11) can also be generalized to describe the resonant decay and spectral cascading of KAWs in, e.g., the solar wind. In this case, the $\omega_{\rm G}$ term, which is unique in toroidal plasmas, can be dropped, and $k_\parallel$ can be taken more flexibly without the periodicity constraint.

We then apply the generic formalism of equation (11) to the parametric decay of a pump RSAE $\boldsymbol{\Omega}_0$ into a RSAE sideband $\boldsymbol{\Omega}_1$ and a BAE $\boldsymbol{\Omega}_{\rm B}$, and taking $\boldsymbol{\Omega}_0=\boldsymbol{\Omega}_1+\boldsymbol{\Omega}_{\rm B}$ as the matching condition without loss of generality. Here, for simplicity, we assume all three SAWs are dominated by single n and m, typical of SAWs excited at $q_{\rm min}$ with large distance between mode rational surfaces,

$$\delta\phi=A\exp\left[-\mathrm{i}(\omega t-n\varphi+m\theta)\right]\Phi(x), \tag{13}$$

where A is the slowly varying amplitude, Φ is the parallel mode structure [55] localized around $q_{\rm min}$, $x\equiv nq-m$, and $\int|\Phi|^2\mathrm{d}x=1$ is taken as normalization condition. Considering $\omega_{\rm B}\sim O(\omega_{\rm ti})$ to maximize the LFAM ion Landau damping, we have $|\omega_0|\simeq|\omega_1|\gg|\omega_{\rm B}|$ and similarly $|k_{\parallel,0}|\simeq|k_{\parallel,1}|\sim O(1/(qR_0))\gg|k_{\parallel,{\rm B}}|$. Thereby, the $q_{\rm min}$ surface actually corresponds to the rational surface of the LFAM, as in the analysis of [49, 50], addressing a case of practical interest for DIII-D [50, 137].

The nonlinear equation for $\boldsymbol{\Omega}_1$ in the WKB limit follows from

$$b_1\mathcal{E}_1\delta\phi_1=-\frac{\mathrm{i}}{\omega_1}\Lambda^{\boldsymbol{k}_1}_{\boldsymbol{k}_0,\boldsymbol{k}_{\rm B^*}}\alpha^{\boldsymbol{k}_1}_{\boldsymbol{k}_0,\boldsymbol{k}_{\rm B^*}}\delta\phi_0\delta\phi_{\rm B^*}, \tag{14}$$

which, after multiplying both sides by Φ_1 and averaging over the fast radial scale, yields the eigenmode dispersion relation of $\boldsymbol{\Omega}_1$,

$$\hat{b}_1\hat{\mathcal{E}}_1A_1=-\frac{\mathrm{i}}{\omega_1}\left\langle\Lambda^{\boldsymbol{k}_1}_{\boldsymbol{k}_0,\boldsymbol{k}_{\rm B^*}}\alpha^{\boldsymbol{k}_1}_{\boldsymbol{k}_0,\boldsymbol{k}_{\rm B^*}}\Phi_1\Phi_0\Phi_{\rm B}\right\rangle_x A_0A_{\rm B^*}, \tag{15}$$

with $\langle\cdots\rangle_x\equiv\int\cdots\mathrm{d}x$ and $(\hat{\cdots})$ denotes weighting over the radial mode structures. Similarly, for the LFAM, one has

$$\hat{b}_{\rm B}\hat{\mathcal{E}}_{\rm B}A_{\rm B}=-\frac{\mathrm{i}}{\omega_{\rm B}}\left\langle\Lambda^{\boldsymbol{k}_{\rm B}}_{\boldsymbol{k}_0,\boldsymbol{k}_1^*}\alpha^{\boldsymbol{k}_{\rm B}}_{\boldsymbol{k}_0,\boldsymbol{k}_1^*}\Phi_{\rm B}\Phi_0\Phi_1\right\rangle_x A_0A_{1^*}. \tag{16}$$

Meanwhile, combining equations (15) and (16), one arrives at the dispersion relation for the RSAE parametric decay

$$\hat{\mathcal{E}}_1\hat{\mathcal{E}}_{\rm B}\simeq\left(\hat{\Lambda}^{\boldsymbol{k}_1}_{\boldsymbol{k}_0,\boldsymbol{k}_{\rm B^*}}\right)^2\frac{\hat{\alpha}_{\rm N}}{\hat{b}_1\hat{b}_{\rm B}\omega_1\omega_{\rm B}}\hat{C}^2|A_0|^2. \tag{17}$$

Here, we note that $\Lambda^{\boldsymbol{k}_1}_{\boldsymbol{k}_0,\boldsymbol{k}_{\rm B^*}}=\Lambda^{\boldsymbol{k}_{\rm B}}_{\boldsymbol{k}_0,\boldsymbol{k}_1^*}$, and define $\hat{\alpha}_{\rm N}\equiv\hat{\alpha}^{\boldsymbol{k}_1}_{\boldsymbol{k}_0,\boldsymbol{k}_{\rm B}^*}\hat{\alpha}^{\boldsymbol{k}_{\rm B}}_{\boldsymbol{k}_0,\boldsymbol{k}_1^*}$, $\hat{C}\equiv\langle\Phi_0\Phi_1\Phi_{\rm B}\rangle_x$, which can be estimated by taking a model profile of Φ. Meanwhile, the mode structure averaged operators are symbolically written here, noting that they are predominantly even with respect to the $q_{\rm min}$ surface. In order to estimate the onset condition for the spontaneous decay, we expand $\hat{\mathcal{E}}_1\simeq(\mathrm{i}\partial_{\omega_1}\hat{\mathcal{E}}_1)(\partial_t+\gamma_1)\simeq(2\mathrm{i}/\omega_1)(\gamma+\gamma_1)$, and similarly $\hat{\mathcal{E}}_{\rm B}\simeq(-2\mathrm{i}/\omega_{\rm B})(\gamma+\gamma_{\rm B})$, with γ the growth rate of the parametric decay instability, γ_1 and $\gamma_{\rm B}$ the respective linear damping rates of $\boldsymbol{\Omega}_1$ and $\boldsymbol{\Omega}_{\rm B}$ from the anti-Hermitian parts of $\hat{\mathcal{E}}$, which are dominated by electron and ion Landau dampings, respectively. Equation (17) then becomes

$$(\gamma+\gamma_1)(\gamma+\gamma_{\rm B})\simeq\left(\hat{\Lambda}^{\boldsymbol{k}_1}_{\boldsymbol{k}_0,\boldsymbol{k}_{\rm B^*}}\right)^2\frac{\hat{\alpha}_{\rm N}}{4\hat{b}_1\hat{b}_{\rm B}}\hat{C}^2|A_0|^2. \tag{18}$$

Thus, the condition for RSAE spontaneous decay can be given as

$$\hat{\alpha}_{\rm N}>0, \tag{19}$$

$$\left(\hat{\Lambda}^{\boldsymbol{k}_1}_{\boldsymbol{k}_0,\boldsymbol{k}_{\rm B^*}}\right)^2\frac{\hat{\alpha}_{\rm N}}{4\hat{b}_1\hat{b}_{\rm B}}\hat{C}^2|A_0|^2>\gamma_1\gamma_{\rm B}, \tag{20}$$

with equation (19) determining the preferred nonlinear couplings in the perpendicular wave-vector space, and equation (20) corresponding to the threshold for the nonlinear drive to overcome the damping of $\boldsymbol{\Omega}_1$ and $\boldsymbol{\Omega}_{\rm B}$.

To gain more insights and shed light on the practical relevance of the present mechanism, we take the WKB limit and enforce the ordering $|k_{\|,\mathrm{B}}| \ll 1/(qR_0)$. In this case, $\hat{\alpha}_\mathrm{N}$ can be reduced to

$$\hat{\alpha}_\mathrm{N} \simeq (b_0-b_1)(b_0-b_1-b_\mathrm{B})\left(1-\frac{k_{\|,0}k_{\|,1}v_\mathrm{A}^2}{\omega_0\omega_1}\right). \tag{21}$$

Still, this expression depends sensitively on both the parallel (related to frequency) and the perpendicular wavenumbers of the three SAWs involved, which determine the scattering direction of the spontaneous decay. Nevertheless, a particular interesting scenario can be identified as the 'normal cascading' of $\boldsymbol{\Omega}_0$ into high-n short wavelength regime, $|k_{\perp,1}| \simeq |k_{\perp,\mathrm{B}}| \gg |k_{\perp,0}|$, where the nonlinear coupling is dominated by the radially fast varying inertial layer. Then, $(b_0-b_1)(b_0-b_1-b_\mathrm{B})>0$ and $1-k_{\|,0}k_{\|,1}v_\mathrm{A}^2/(\omega_0\omega_1)>0$ could also be satisfied if $\boldsymbol{\Omega}_1$ resides above the SAW CAP, which may be achieved noting the potentially dense RSAE/KRSAE spectrum in burning plasmas. Note also that the LHS of equation (20) is proportional to b_1, and thus, it also favors the normal cascading scenario. The scattering to large $|k_{\perp,1}| \gg |k_{\perp,0}|$, high-$n_1$ region indicates stronger symmetry breaking, and thus, more significant resonant particle transport. The threshold on the pump RSAE amplitude can be estimated as $\delta B_{\perp,0}^2/B_0^2 \gtrsim (10^{-7})$ assuming typical plasma parameters [43].

Another important implication of the present mechanism is the collisionless ion heating via the fuel ion Landau damping of the nonlinearly generated LFAM. To give an order of magnitude estimation of the heating rate, we consider the feedback of the sidebands to the RSAE pump wave,

$$\hat{b}_0\hat{\mathcal{E}}_0 A_0 = -\frac{\mathrm{i}}{\omega_0}\hat{\Lambda}^{k_0}_{k_1,k_\mathrm{B}}\hat{\alpha}^{k_0}_{k_1,k_\mathrm{B}}\hat{C}A_1A_\mathrm{B}\,. \tag{22}$$

Using local expansions of $\hat{\mathcal{E}}$ in equations (15), (16), (22), one obtains the coupled three wave equations,

$$(\partial_t+\gamma_1)A_1 = -\frac{\hat{\alpha}^{k_1}_{k_0,k_{\mathrm{B}^*}}}{\hat{b}_1\omega_1\partial_{\omega_1}\mathcal{E}_{1,\mathfrak{R}}}\hat{\Lambda}^{k_1}_{k_0,k_{\mathrm{B}^*}}\hat{C}A_0A_{\mathrm{B}^*}\,, \tag{23}$$

$$(\partial_t+\gamma_\mathrm{B})A_\mathrm{B} = -\frac{\hat{\alpha}^{k_\mathrm{B}}_{k_0,k_1^*}}{\hat{b}_\mathrm{B}\omega_\mathrm{B}\partial_{\omega_\mathrm{B}}\mathcal{E}_{\mathrm{B},\mathfrak{R}}}\hat{\Lambda}^{k_\mathrm{B}}_{k_0,k_1^*}\hat{C}A_0A_{1^*}\,, \tag{24}$$

$$(\partial_t-\gamma_0)A_0 = -\frac{\hat{\alpha}^{k_0}_{k_1,k_\mathrm{B}}}{\hat{b}_0\omega_0\partial_{\omega_0}\mathcal{E}_{0,\mathfrak{R}}}\hat{\Lambda}^{k_0}_{k_1,k_\mathrm{B}}\hat{C}A_1A_\mathrm{B}\,. \tag{25}$$

Possible solutions of this coupled driven-dissipative system include fixed point attractor, limited cycle oscillation, or even period doubling route to chaos [138]. Here, we give an order of magnitude estimation of the saturation level of A_B from fixed point solution of equations (23) and (25), which is then used give the ion heating rate as

$$\begin{aligned} P_\mathrm{i} &= 2\gamma_\mathrm{B}\omega_\mathrm{B}\partial_{\omega_\mathrm{B}}\mathcal{E}_{\mathrm{B},\mathfrak{R}}\frac{n_\mathrm{i}e^2}{T_\mathrm{i}}\hat{b}_\mathrm{B}|A_\mathrm{B}|^2 \\ &\simeq 10^{-3}\gamma_0 n_\mathrm{i}T_\mathrm{i}\,, \end{aligned} \tag{26}$$

where threshold estimate for the RSAE pump decay intensity of $|\delta B_{\perp,0}|^2/B_0^2 \gtrsim (10^{-7})$ given above was used. Taking $\gamma/\omega \sim O(10^{-2})$ as a typical ordering (e.g., from figure 3(b)), this shows that the fuel ion heating power density could be comparable to the expected alpha particle power in burning plasmas, $P \sim nT/\tau_\mathrm{E}$, with τ_E the energy confinement time typically of the order of seconds. Thus, the present heating mechanism via LFAM collisionless damping is expected to be a possibly important supplement to the alpha channeling process in burning plasmas. Note also that the secondary LFAM has a narrower extent than the pump RSAE, thus, the deposited power will be strictly localized around q_min surface in the core region.

3.3. Modulational instability and the generation of ZFZS

The spontaneous excitation of ZFZS by a pump wave was firstly considered for drift and drift-Alfvén waves as a paradigm case [131], and then extended for TAE [51] and BAE [139]. It was shown that for the TAE, the generation of zonal magnetic field, i.e., zonal current (ZC) is dominant over the electrostatic zonal flow (ZF), mainly due to the magnetically trapped-ion enhanced polarizability [62]. However, for the BAE with $|k_\| v_\mathrm{A}/\omega| \simeq 0$, the MX reflecting the electron response becomes much smaller than the RS for ions, and the generation of fine radial scale ZF is preferred [139]. For the RSAE, the analysis mainly follows from a similar argument [52]. The waves in the nonlinear coupling include the RSAE pump wave $\boldsymbol{\Omega}_0(\omega_0,\boldsymbol{k}_0)$ described by the ballooning mode decomposition [55],

$$\delta\phi_0 = A_0\mathrm{e}^{\mathrm{i}(-\omega_0 t+n\varphi-m_0\theta)}\sum_j \mathrm{e}^{-\mathrm{i}j\theta}\Phi_\mathrm{o}(x-j)+\mathrm{c.c.}\,, \tag{27}$$

the zonal fields $\boldsymbol{\Omega}_\mathrm{z}(\omega_\mathrm{z},\boldsymbol{k}_\mathrm{z})$,

$$\delta\phi_\mathrm{z} = A_\mathrm{z}\mathrm{e}^{-\mathrm{i}\omega_\mathrm{z}t+\mathrm{i}\int k_\mathrm{z}\mathrm{d}r}\sum_j \Phi_\mathrm{z}(x-j)+\mathrm{c.c.}\,, \tag{28}$$

with, noting that the zonal fields are characterized by $n=0$, summation over j denoting the radial structure due to RSAE poloidal harmonics; and the upper/lower sidebands induced by the ZFZSs' feedback to the pump wave, $\boldsymbol{\Omega}_\pm(\omega_\pm,\boldsymbol{k}_\pm)$,

$$\begin{aligned} \delta\phi_\pm = A_\pm\mathrm{e}^{\pm\mathrm{i}(-\omega_\pm t+n\varphi-m_0\theta)}\mathrm{e}^{\mathrm{i}\left(-\omega_\mathrm{z}t+\int k_\mathrm{z}\mathrm{d}r\right)} \\ \times\sum_j \mathrm{e}^{\mp\mathrm{i}j\theta}\left\{\begin{array}{c}\Phi_\mathrm{o}(x-j)\\ \Phi_\mathrm{o}^*(x-j)\end{array}\right\}+\mathrm{c.c.}\,. \end{aligned} \tag{29}$$

Similar forms for $\delta\psi$ are assumed and the frequency and wavenumber matching conditions are implied. Here, consistent with the previous treatments [139], the ZFZSs are assumed to contain a fine-scale radial structure in Φ_z, denoted by the summation over j in equation (28), in addition to the well-known meso-scale envelope in k_z.

Nonlinear equation for the ZF generation can be derived from the surface averaged vorticity equation (3),

$$\omega_\mathrm{z}\hat{\chi}_\mathrm{z}\delta\phi_\mathrm{z} = -\mathrm{i}\frac{c}{B_0}k_\mathrm{z}k_{\theta,0}\left(1-\frac{k_{\|,0}^2v_\mathrm{A}^2}{\omega_0^2}\right)(A_+A_0^*-A_-A_0)\,. \tag{30}$$

Here, $\hat{\chi_z} = \chi_z/(k_z\rho_i)^2 \simeq 1.6q^2\epsilon^{-1/2}$ is the magnetically trapped-ion enhanced polarizability [62]. The finite factor $\propto (1-k_{\|,0}^2 v_A^2/\omega_0^2)$ denotes the breaking of pure Alfvénic state for discrete AEs, and, in the specific RSAE case considered here, by the q-curvature; i.e., $\partial_r^2 q$ at $q_{\min}$. Here, we have neglected the EP's nonperturbative effect by letting Φ_0 being purely real. Interested readers may refer to [124, 140] for an extension to more general cases where resonant EP contribution may render the ZF generation to a 'forced-driven' process. Meanwhile, the generation of ZC follows from equation (5),

$$\delta\psi_z = \mathrm{i}\frac{c}{B_0}\frac{k_z k_{\theta,0}}{\omega_0}\left(A_+ A_0^* - A_- A_0\right). \tag{31}$$

On the other hand, when considering the modulation of ZFZS to the pump RSAE, the equations for the sidebands can be derived from equations (3) and (5) as [52, 139]

$$\begin{aligned} k_{\perp,\pm}^2 \mathcal{E}_\pm \delta\phi_\pm = -\mathrm{i}\frac{c}{B_0\omega_\pm}\left(k_z^2 - k_{\theta,0}^2 - \frac{k_{\|,0}^2 v_A^2}{\omega_0^2}k_{\perp,\pm}^2\right) \\ \times k_z k_{\theta,0}\left\{\begin{array}{c}\delta\phi_0\\ \delta\phi_0^*\end{array}\right\}\left(\delta\phi_z - \alpha\delta\psi_z\right). \end{aligned} \tag{32}$$

Here, $\mathcal{E}$ takes the form of equation (8) in the local WKB limit. The coupling coefficient

$$\alpha \equiv \frac{-2k_{\theta,0}^2 k_{\|,0}^2 v_A^2/\omega_0^2}{k_z^2 - k_\theta^2 - k_{\perp,0}^2 k_{\|,0}^2 v_A^2/\omega_0^2},$$

depends sensitively on the linear properties of the pump RSAE, with a particular important role played by the $|k_{\|,0}v_A/\omega_0|$ value. For a RSAE close to the TAE frequency range, $|k_{\|,0}| \simeq 1/(2qR_0)$ and $|k_{\|,0}v_A/\omega_0| \simeq 1$, one has $\alpha \simeq 1$ [51]. Instead, for a BAE-like RSAE with $|k_{\|,0}v_A/\omega_0| \ll 1$, $\alpha \ll 1$ instead [139]. Combining equations (30)–(32), we finally arrive at the dispersion relation for the modulational instability,

$$\begin{aligned} 1 = \hat{F}|\delta\phi_0|^2\left[\left(\frac{1-k_{\|,0}^2 v_A^2/\omega_0^2}{\omega_z\hat{\chi}_z} + \frac{\alpha}{\omega_0}\right)\frac{1}{\mathcal{E}_+}\right. \\ \left. -\left(\frac{1-k_{\|,0}^2 v_A^2/\omega_0^2}{\omega_z\hat{\chi}_z} - \frac{\alpha}{\omega_0}\right)\frac{1}{\mathcal{E}_-}\right], \end{aligned} \tag{33}$$

with

$$\hat{F} = \left(\frac{ck_z k_{\theta,0}}{B_0}\right)^2 \frac{k_z^2 - k_{\theta,0}^2 - k_{\perp,\pm}^2 k_{\|,0}^2 v_A^2/\omega_0^2}{k_{\perp,\pm}^2\omega_0},$$

the nonlinear coupling coefficient and $k_{\perp,\pm}^2 = k_{\perp,0}^2 + k_z^2$. By expanding $\mathcal{E}_\pm$ locally about the RSAE dispersion relation, $\mathcal{E}_\pm \simeq (\partial\mathcal{E}_0/\partial\omega_0)(\pm\omega_z - \Delta)$, with

$$\Delta \equiv k_z^2 \frac{\partial^2\mathcal{E}_0/\partial k_r^2}{2\partial\mathcal{E}_0/\partial\omega_0}, \tag{34}$$

the frequency mismatch of the sidebands due to ZFZS modulation, and letting $\omega_z \equiv \mathrm{i}\gamma_z$, equation (33) can be written as

$$\gamma_z^2 = -\Delta^2 + \frac{2\hat{F}|\delta\phi_0|^2}{\partial\mathcal{E}_0/\partial\omega_0}\left(-\frac{1-k_{\|,0}^2 v_A^2/\omega_0^2}{\hat{\chi}_z} + \frac{\alpha}{\omega_0}\Delta\right). \tag{35}$$

Equation (35) essentially summarizes the most interesting features of ZFZS excited by the RSAE modulational instability. The first term on the RHS corresponds to the threshold due to the frequency mismatch, while the second term is the nonlinear drive associated with the pump RSAE amplitude. The threshold condition can be estimated to be $\delta B_\theta/B_0 \sim O(10^{-4})$ for typical plasma parameters [52], similar to the cases of TAE [51] and BAE [139], and slightly lower than the parametric decay instability in section 3.2. Moreover, the two terms in the parentheses correspond to the nonlinear drive to ZF and ZC, respectively. One sees that the previous results for TAE [51] and BAE [139] are well recovered in the appropriate limits. The ZC is preferentially excited when the RSAE is in the TAE frequency range and $\Delta > 0$. On the other hand, the drive to ZF is generally weak due to the neoclassical polarizability effect, unless $|k_\| v_A/\omega| \simeq 0$ and the RSAE is close to a BAE. In any case, the spontaneously generated ZFZSs could interact with DW turbulence and regulate the anomalous transport in the plasma core.

The above treatment considers the 'linear' growth stage of the modulational instability. For the strongly nonlinear stage where the feedback of daughter waves to the RSAE pump wave is significant, equations (30)–(32) could also be generalized without separating the sidebands from the pump wave, as [52]

$$\begin{aligned} k_{\perp,0}^2\mathcal{E}_0\delta\phi_0 = -\left(\frac{ck_z k_{\theta,0}}{B_0}\right)^2\frac{1}{\omega_0}\left(k_z^2 - k_{\theta,0}^2 - \frac{k_{\|,0}^2 v_A^2}{\omega_0^2}k_{\perp,0}^2\right) \\ \times\left[\frac{1-k_{\|,0}^2 v_A^2/\omega_0^2}{\omega_z\hat{\chi}_z k_z}\left(k_{r,0} - k_{r,0}^*\right) + \frac{\alpha}{\omega_0}\right]|\delta\phi_0|^2\delta\phi_0. \end{aligned} \tag{36}$$

This dispersion relation could be solved numerically as an initial value problem of the coupled pump-ZFZS system [141, 142]. Here, in order to make analytical progress and give an order of magnitude estimation on the saturation amplitudes, we consider the 'TAE-limit', where the generation of ZC is dominant, and perturbatively expand $\mathcal{E}_0 \simeq (\partial\mathcal{E}_0/\partial\omega_0)\times(\mathrm{i}\partial_t - \Delta)$, with Δ given by equation (34) and denoting the nonlinear frequency shift. Equation (36) can then be reduced to

$$\left[\mathrm{i}\partial_t - \Delta - 2\left(\frac{c}{B_0\omega_0}k_z k_{\theta,0}\right)^2\frac{|\delta\phi_0|^2}{\partial\mathcal{E}_0/\partial\omega_0}\right]\delta\phi_0 = 0, \tag{37}$$

i.e., a nonlinear equation describing the time evolution of $\delta\phi_0$ including the nonlinear scattering to nearby eigenstates and the self-modulation by the ZFZS generation. To estimate the saturation amplitude as a fixed point solution, corresponding to the pump wave being scattered into stable eigenstates by the self-consistently generated ZFZS, we take the balance of the frequency shift and modulation terms in equation (37), as

$$|\delta\phi_0|^2 = \frac{\partial^2\mathcal{E}_0}{\partial k_r^2}\left(\frac{B_0\omega_0}{2ck_{\theta,0}}\right)^2. \tag{38}$$

Using typical tokamak parameters, equation (38) gives a rough ordering of the RSAE saturation amplitude $\delta B_\theta/B \sim O(10^{-4})$, which is of the same order of the typically observed RSAE amplitude driven by EP as well as of the estimated onset threshold from equation (35). Note that in the above estimation, we only focus on the pump RSAE and do not explicitly consider the nonlinear distortion of the MHD equilibrium. However, the generated ZC itself is a corrugation of the equilibrium magnetic field nearby $q_{\min}$, and we have $\delta q/q \sim O(10^{-3})$ from the above ordering. Noting the unique sensitivity of the RSAE spectrum to a small variation of $q_{\min}$ at high n, equation (38) denotes a rough saturation criteria as the local modulation of SAW continuum is comparable to the frequency mismatch between RSAE and SAW CAP. Thus, the generation of ZC may provide a novel saturation mechanism for the RSAE via, simultaneously, scattering the RSAE pump wave in both frequency and wavenumber domains and local distortion of the SAW continuum [52]. This is conceptually analogous to references [121, 122] which analyze the TAE saturation by enhanced damping via continuum distortion in the MHD regime. In future works, it would be interesting to investigate the saturation mechanism more self-consistently by considering both nonlinear effects on the same footing, where the global RSAE dispersion relation [7] is fully accounted for.

4. Conclusion, discussion and outlook

In this paper, we review several key nonlinear dynamics of the $n \sim O(10)$ reversed shear Alfvén eigenmode excited by energetic particles in the core of burning plasmas. Guided by the general theoretical framework [2] and the relevant nonlinear physics, the analyses are further subdivided into the wave-particle resonant interaction and the wave-wave coupling adopting different approaches as needed. Using simplified hybrid MHD-kinetic simulations, the structures of phase space resonance for both trapped and circulating EP with the RSAE are illustrated. It is shown that the radial resonance width is typically broad and comparable with the radial width of the RSAE. This property indicates that, in order to reach saturation,the resonant EP radial redistribution scale must be comparable with the radial mode width and EP radially decouple from the localized RSAE mode structure. The resultant resonant EP transport induced by a RSAE is nonlocal, generally coherent, and contains a significant convective component. Effectively, the core-localized RSAEs could pump out EP to the outer-core region, and may lead to global cross-region interactions with, e.g., the TAEs.

Further to this, two channels of nonlinear mode couplings are studied by the nonlinear gyrokinetic theory, considering the spontaneous decay of a finite amplitude pump RSAE as an application. It is shown that many RSAEs as well as kinetic RSAEs with radially overlapped mode structure and closely separated frequencies may couple together and generate a low frequency Alfvénic mode. In addition to spectral cascading and mode conversion to short wavelength kinetic fluctuations, this decay channel may lead to the spectral energy transfer to LFAM, which could efficiently heat thermal ions via collisionless damping. Thereby, the parametric decay of RSAE may serve as a supplementary core-localized alpha channeling mechanism by transferring EP energy to fuel ions. A finite amplitude RSAE could also spontaneously excite the zero frequency zonal field structures via modulational instability, including both zonal current and zonal flow. The previous studies on the TAE [51] and BAE [139] are well recovered as limiting cases, and the branching ratio of the ZC versus ZF is shown to be mainly determined by the pump RSAE's frequency range, i.e., its closeness to the TAE or BAE limits. It is shown that, in the 'T AE limit' where the generation of ZC prevails, the estimated ZC level could locally distort to the continuum structure around RSAE location, and thus, provide a novel and effective saturation channel for the RSAE.

The concept of 'saturation' is discussed throughout this article in various aspects, emphasizing that the related theoretical study and experimental validation is still an active research field. Indeed, all three nonlinear channels discussed here could lead to the saturation of an unstable mode, as either a weakening of external EP drive or an increased wave damping by spectral energy transfer. In this work, this complication is treated by separately inspecting the relevant physics and spatiotemporal scales. For example, in section 2, we mainly focus on the wave-EP resonant dynamics taking place on the mesoscales of the order of the EP orbit width, which is relatively very fast, from the linear growth stage to the initial saturation where significant EP transport takes place. While in section 3, we start from this initial saturation point and explore the mode's further evolution by wave-wave couplings dominated by short radial scale scattering. In practice, such timescale separation may not be strictly valid, as some nearly thresholdless forced driven mode coupling processes could take place in the linear growth stage [124, 143], including the excitation of ZFZS and LFAM. Thus, a thorough and quantitative investigation of the RSAE saturation and its impact on particle transport and fusion performance naturally requires taking both routes to the nonlinear physics into consideration on the same footing [2, 58, 68]. This is of particular importance but extremely channeling for either analytical theory [140] or global gyrokinetic simulations [144, 145]. A viable route to tackle the difficulty of this multi-scale, multi-physics problem could be provided by the phase space zonal structure theoretical framework [2, 68, 69, 108, 119], which describes the nonlinear wave-particle interaction using coupled Dyson-Schrödinger model equations and could be naturally extended to nonlinear wave-wave couplings in the form of nonlinear radial envelope equations.

In the theoretical analyses of the nonlinear mode coupling, to simplify the analytical derivation, we mostly neglect the effect of plasma nonuniformity by considering the local WKB limit of the RSAE dispersion relation. Including the plasma nonuniformity would introduce the diamagnetic effect and the structure of the SAW continuum,

allowing us to generalize the present analysis to the cases of KBM and AITG. One may also self-consistently study the RSAE saturation via the self-generated ZC. Such an extension could be tedious but straightforward. Some recent analyses [132, 146] have already begun to explore possible interesting implications of these physics.

We finally discuss some future research topics that stem from the present analysis. Although the EP transport by a single RSAE is predominantly convective, many other effects, such as overlapped resonances by multiple modes [147] or background turbulences [148], may break such coherent phase space structures and possibly render the long timescale EP transport diffusive. Thus, a proper characterization of long timescale EP confinement should include more physics gradients beyond the present simplified study. In fact, both diffusive [149] and coherent [109] types of EP flow have been reported experimentally, implying that quantitative prediction should be explored case-by-case. Another factor neglected in the present work is the interplay with universal microscopic turbulences, despite that the spontaneously generated ZFZSs are bound to have an intense interactions with them [53]. This is a broad and intense research field, which has recently drawn significant research attentions on the cross scale interactions between AEs and turbulences as either direct coupling [150, 151], or indirect interaction via ZFZS [54, 152–154] or the EP phase space structures [54, 145, 152, 153]. All these complications demonstrate that the reactor-grade burning plasma is inherently a complex multi-scale system [2, 54], where the RSAE might play a central role.

Acknowledgments

The authors are in debt to many collaborators who contributed to the original works and provided fruitful comments and discussions. This work is supported by National Natural Science Foundation of China (Nos. 12205251, 12275236 and 12261131622), Italian Ministry for Foreign Affairs and International Cooperation Project (No. CN23GR02), the National Key Research and Development Program of China (Nos. 2019YFE03020003 and 2017YFE0301900), and 'Users of Excellence program of Hefei Science Center CAS (No. 2021HSC-UE016)'. This work has been carried out within the framework of the EUROfusion Consortium, funded by the European Union via the Euratom Research and Training Programme (No. 101052200–EUROfusion). Views and opinions expressed are however those of the author(s) only and do not necessarily reflect those of the European Union or the European Commission. Neither the European Union nor the European Commission can be held responsible for them.

References

[1] Alfvén H 1942 *Nature* **150** 405
[2] Chen L and Zonca F 2016 *Rev. Mod. Phys.* **88** 015008
[3] Heidbrink W W *et al* 2007 *Phys. Rev. Lett.* **99** 245002
[4] Ding R *et al* 2015 *Nucl. Fusion* **55** 023013
[5] Fasoli A *et al* 2007 *Nucl. Fusion* **47** S264
[6] Sharapov S E *et al* 2002 *Phys. Plasmas* **9** 2027
[7] Zonca F *et al* 2002 *Phys. Plasmas* **9** 4939
[8] Grad H 1969 *Physics Today* **22** 34
[9] Chen L and Hasegawa A 1974 *Phys. Fluids* **17** 1399
[10] Hasegawa A and Chen L 1976 *Phys. Fluids* **19** 1924
[11] Chen L, Zonca F and Lin Y 2021 *Rev. Mod. Plasma Phys.* **5** 1
[12] Chen L 1994 *Phys. Plasmas* **1** 1519
[13] Cheng C Z, Chen L and Chance M S 1985 *Ann. Phys.* **161** 21
[14] Kieras C E and Tataronis J A 1982 *J. Plasma Phys.* **28** 395
[15] Heidbrink W W *et al* 1993 *Phys. Rev. Lett.* **71** 855
[16] Zonca F, Chen L and Santoro R A 1996 *Plasma Phys. Control. Fusion* **38** 2011
[17] Mett R R and Mahajan S M 1992 *Phys. Fluids B* **4** 2885
[18] Zonca F and Chen L 1996 *Phys. Plasmas* **3** 323
[19] Zonca F and Chen L 2014 *Phys. Plasmas* **21** 072120
[20] Zonca F and Chen L 2014 *Phys. Plasmas* **21** 072121
[21] Wang X, Zonca F and Chen L 2010 *Plasma Phys. Control. Fusion* **52** 115005
[22] Kimura H *et al* 1998 *Nucl. Fusion* **38** 1303
[23] Takechi M *et al* 2005 *Phys. Plasmas* **12** 082509
[24] Breizman B N *et al* 2003 *Phys. Plasmas* **10** 3649
[25] Berk H L *et al* 2001 *Phys. Rev. Lett.* **87** 185002
[26] Fu G Y and Berk H L 2006 *Phys. Plasmas* **13** 052502
[27] Gorelenkov N N 2008 *Phys. Plasmas* **15** 110701
[28] Deng W J *et al* 2010 *Phys. Plasmas* **17** 112504
[29] Huang J *et al* 2020 *Nucl. Fusion* **60** 126007
[30] Heidbrink W W *et al* 2013 *Phys. Plasmas* **20** 082504
[31] Chen W *et al* 2014 *Nucl. Fusion* **54** 104002
[32] Dreval M *et al* 2022 *Nucl. Fusion* **62** 056001
[33] Breizman B N and Sharapov S E 2011 *Plasma Phys. Control. Fusion* **53** 054001
[34] Shimada M *et al* 2007 *Nucl. Fusion* **47** S1
[35] Wan Y X *et al* 2017 *Nucl. Fusion* **57** 102009
[36] Creely A J *et al* 2020 *J. Plasma Phys.* **86** 865860502
[37] Fisch N J 2000 *Nucl. Fusion* **40** 1095
[38] Gormezano C *et al* 2007 *Nucl. Fusion* **47** S285
[39] Sauter O, Angioni C and Lin-Liu Y R 1999 *Phys. Plasmas* **6** 2834
[40] Wang T *et al* 2018 *Phys. Plasmas* **25** 062509
[41] Wang T *et al* 2019 *Phys. Plasmas* **26** 012504
[42] Wang T *et al* 2020 *Nucl. Fusion* **60** 126032
[43] Wei S Z *et al* 2022 *Nucl. Fusion* **62** 126038
[44] Chen L and Zonca F 2017 *Phys. Plasmas* **24** 072511
[45] Falessi M V *et al* 2020 *J. Plasma Phys.* **86** 845860501
[46] Tsai S T and Chen L 1993 *Phys. Fluids B* **5** 3284
[47] Zonca F *et al* 1998 *Plasma Phys. Control. Fusion* **40** 2009
[48] Zonca F *et al* 1999 *Phys. Plasmas* **6** 1917
[49] Ma R R *et al* 2022 *Plasma Phys. Control. Fusion* **64** 035019
[50] Ma R R *et al* 2023 *Phys. Plasmas* **30** 042105
[51] Chen L and Zonca F 2012 *Phys. Rev. Lett.* **109** 145002
[52] Wei S Z *et al* 2021 *J. Plasma Phys.* **87** 905870505
[53] Lin Z H *et al* 1998 *Science* **281** 1835
[54] Zonca F *et al* 2015 *Plasma Phys. Control. Fusion* **57** 014024
[55] Connor J W, Hastie R J and Taylor J B 1978 *Phys. Rev. Lett.* **40** 396
[56] Biglari H and Chen L 1991 *Phys. Rev. Lett.* **67** 3681
[57] Chen L and Zonca F 2011 *EPL* **96** 35001
[58] Chen L and Zonca F 2013 *Phys. Plasmas* **20** 055402
[59] Park W *et al* 1992 *Phys. Fluids B* **4** 2033
[60] Briguglio S *et al* 1995 *Phys. Plasmas* **2** 3711
[61] Frieman E A and Chen L 1982 *Phys. Fluids* **25** 502
[62] Rosenbluth M N and Hinton F L 1998 *Phys. Rev. Lett.* **80** 724

[63] Sagdeev R Z and Galeev A A 1969 *Nonlinear Plasma Theory* (New York: Benjamin)
[64] Wei S Z *et al* 2021 *Chin. Phys. Lett.* **38** 035201
[65] Berk H L and Breizman B N 1990 *Phys. Fluids B* **2** 2226
[66] Berk H L and Breizman B N 1990 *Phys. Fluids B* **2** 2235
[67] Berk H L and Breizman B N 1990 *Phys. Fluids B* **2** 2246
[68] Zonca F *et al* 2015 *New J. Phys.* **17** 013052
[69] Falessi M V and Zonca F 2019 *Phys. Plasmas* **26** 022305
[70] Zhang H S, Lin Z H and Holod I 2012 *Phys. Rev. Lett.* **109** 025001
[71] Wang X *et al* 2012 *Phys. Rev. E* **86** 045401(R)
[72] Yu L M *et al* 2022 *EPL* **138** 54002
[73] Todo Y and Sato T 1998 *Phys. Plasmas* **5** 1321
[74] Fu G Y *et al* 2006 *Phys. Plasmas* **13** 052517
[75] Zhu J, Ma Z W and Wang S 2016 *Phys. Plasmas* **23** 122506
[76] Chen L, White R B and Rosenbluth M N 1984 *Phys. Rev. Lett.* **52** 1122
[77] Zonca F, *et al* 2005 *Nucl. Fusion* **45** 477
[78] Tobias B J *et al* 2011 *Phys. Rev. Lett.* **106** 075003
[79] Briguglio S, Zonca F and Vlad G 1998 *Phys. Plasmas* **5** 3287
[80] Vlad G, Zonca F and Briguglio S 1999 *Riv. Nuovo Cim.* **22** 1
[81] Izzo R *et al* 1983 *Phys. Fluids* **26** 2240
[82] Breizman B N *et al* 2005 *Phys. Plasmas* **12** 112506
[83] Hahm T S, Lee W W and Brizard A 1988 *Phys. Fluids* **31** 1940
[84] Chew G F, Goldberger M L and Low F E 1956 *Proc. Roy. Soc. London Ser. A Math. Phys. Sci.* **236** 112
[85] Albanese R *et al* 2017 *Fusion Eng. Des.* **122** 274
[86] Stix T H 1972 *Plasma Phys.* **14** 367
[87] Pizzuto A *et al* 2010 *Nucl. Fusion* **50** 095005
[88] Vlad G *et al* 2013 *Nucl. Fusion* **53** 083008
[89] Spong D A 2013 *Nucl. Fusion* **53** 053008
[90] Yang Y R *et al* 2020 *Nucl. Fusion* **60** 106012
[91] Briguglio S *et al* 2014 *Phys. Plasmas* **21** 112301
[92] Zonca F *et al* 2007 *Nucl. Fusion* **47** 1588
[93] Fu G Y and Cheng C Z 1992 *Phys. Fluids B* **4** 3722
[94] Chen L 1988 *Theory of Fusion Plasmas* edited by J. Vaclavik and F. Troyon and E. Sindoni, Association EURATOM, Bologna, Italy, p 327
[95] Fu G Y and Van Dam J W 1989 *Phys. Fluids B* **1** 1949
[96] Pinches S D *et al* 2015 *Phys. Plasmas* **22** 021807
[97] Lauber P 2015 *Plasma Phys. Control. Fusion* **57** 054011
[98] Schneller M, Lauber P and Briguglio S 2016 *Plasma Phys. Control. Fusion* **58** 014019
[99] Rodrigues P *et al* 2015 *Nucl. Fusion* **55** 083003
[100] Fitzgerald M *et al* 2016 *Nucl. Fusion* **56** 112010
[101] White R B 2012 *Commun. Nonlinear Sci. Numer. Simulat.* **17** 2200
[102] Briguglio S *et al* 2017 *Nucl. Fusion* **57** 072001
[103] Wang X *et al* 2016 *Phys. Plasmas* **23** 012514
[104] Hsu C T and Sigmar D J 1992 *Phys. Fluids B* **4** 1492
[105] White R B *et al* 1983 *Phys. Fluids* **26** 2958
[106] Heidbrink W W and White R B 2020 *Phys. Plasmas* **27** 030901
[107] Berk H L, Breizman B N and Pekker M 1996 *Phys. Rev. Lett.* **76** 1256
[108] Zonca F *et al* 2021 *J. Phys.: Conf. Ser.* **1785** 012005
[109] Du X D *et al* 2021 *Phys. Rev. Lett.* **127** 235002
[110] Shinohara K *et al* 2001 *Nucl. Fusion* **41** 603
[111] Shinohara K *et al* 2004 *Plasma Phys. Control. Fusion* **46** S31
[112] Sharapov S E *et al* 2006 *Nucl. Fusion* **46** S868
[113] Bierwage A, White R B and Duarte V N 2021 *Plasma Fusion Res.* **16** 1403087
[114] Wang X *et al* 2022 *Phys. Plasmas* **29** 032512
[115] Briguglio S *et al* 2007 *Phys. Plasmas* **14** 055904
[116] Bierwage A *et al* 2013 *Nucl. Fusion* **53** 073007
[117] White R B *et al* 2010 *Phys. Plasmas* **17** 056107
[118] White R B *et al* 2010 *Plasma Phys. Control. Fusion* **52** 045012
[119] Falessi M V *et al* 2023 *New J. Phys.* **25** 123035
[120] Hahm T S and Chen L 1995 *Phys. Rev. Lett.* **74** 266
[121] Chen L *et al* 1998 *Plasma Phys. Control. Fusion* **40** 1823
[122] Zonca F *et al* 1995 *Phys. Rev. Lett.* **74** 698
[123] Qiu Z Y, Chen L and Zonca F 2013 *EPL* **101** 35001
[124] Qiu Z Y, Chen L and Zonca F 2016 *Phys. Plasmas* **23** 090702
[125] Qiu Z Y, Chen L and Zonca F 2019 *Nucl. Fusion* **59** 066024
[126] Qiu Z Y *et al* 2019 *Nucl. Fusion* **59** 066031
[127] Wei S Z *et al* 2019 *Phys. Plasmas* **26** 074501
[128] Qiu Z Y, Chen L and Zonca F 2023 *Rev. Mod. Plasma Phys.* **7** 28
[129] Chen L, Lin Z H and White R 2000 *Phys. Plasmas* **7** 3129
[130] Chen L and Hasegawa A 1991 *J. Geophys. Res.* **96** 1503
[131] Chen L *et al* 2001 *Nucl. Fusion* **41** 747
[132] Chen L, Qiu Z Y and Zonca F 2022 *Phys. Plasmas* **29** 050701
[133] Winsor N, Johnson J L and Dawson J M 1968 *Phys. Fluids* **11** 2448
[134] Zonca F and Chen L 2008 *EPL* **83** 35001
[135] Qiu Z Y, Chen L and Zonca F 2018 *Plasma Sci. Technol.* **20** 094004
[136] Conway G D, Smolyakov A I and Ido T 2022 *Nucl. Fusion* **62** 013001
[137] Heidbrink W W *et al* 2021 *Nucl. Fusion* **61** 016029
[138] Russell D A, Hanson J D and Ott E 1980 *Phys. Rev. Lett.* **45** 1175
[139] Qiu Z Y, Chen L and Zonca F 2016 *Nucl. Fusion* **56** 106013
[140] Qiu Z Y, Chen L and Zonca F 2017 *Nucl. Fusion* **57** 056017
[141] Guo Z H, Chen L and Zonca F 2009 *Phys. Rev. Lett.* **103** 055002
[142] Chen N F *et al* 2022 *Plasma Phys. Control. Fusion* **64** 015003
[143] Todo Y, Berk H L and Breizman B N 2010 *Nucl. Fusion* **50** 084016
[144] Biancalani A *et al* 2021 *Plasma Phys. Control. Fusion* **63** 065009
[145] Liu P *et al* 2022 *Phys. Rev. Lett.* **128** 185001
[146] Wang Y H *et al* 2022 *J. Plasma Phys.* **88** 895880601
[147] Chirikov B V 1979 *Phys. Rep.* **52** 263
[148] Zhang W L, Lin Z H and Chen L 2008 *Phys. Rev. Lett.* **101** 095001
[149] Collins C S *et al* 2016 *Phys. Rev. Lett.* **116** 095001
[150] Chen L, Qiu Z Y and Zonca F 2022 *Nucl. Fusion* **62** 094001
[151] Chen L, Qiu Z Y and Zonca F 2023 *Nucl. Fusion* **63** 106016
[152] Zonca F *et al* 2006 *Plasma Phys. Control. Fusion* **48** B15
[153] Chen L and Zonca F 2007 *Nucl. Fusion* **47** S727
[154] Mazzi S *et al* 2022 *Nat. Phys.* **18** 776